

Review

Metal Oxide-Based Sensors for Ecological Monitoring: Progress and Perspectives

Mykhail Tereshkov¹, Tetiana Dontsova¹, Bilge Saruhan²  and Svitlana Krüger^{2,*} 

¹ Faculty of Chemical Technology, Department of Technologies Inorganic Substances, Water Treatment and General Chemical Technology, National Technical University of Ukraine “Igor Sikorsky Kyiv Polytechnic Institute”, 37/4, Prospect Beresteiskyi, 03056 Kyiv, Ukraine; m.tereshkov@xtf.kpi.ua (M.T.); t.dontsova@kpi.ua (T.D.)

² Institute of Materials Research, German Aerospace Center (DLR), Linder Hoehe, 51147 Cologne, Germany; bilge.saruhan@dlr.de

* Correspondence: svitlana.krueger@dlr.de

Abstract: This paper aims to provide a large coverage of recent developments regarding environmental monitoring using metal oxide-based sensors. Particular attention is given to the detection of gases such as H₂, CO_x, SO_x, NO_x, and CH₄. The developments and analyses of the design of sensors and types of metal oxide sensing materials are emphasized. The sensing mechanisms and peculiarities of metal oxides used in chemoresistive sensors are provided. The main parameters that affect the sensitivity and selectivity of metal oxide sensors are indicated and their significance to the sensor signal is analyzed. Modern data processing algorithms, employed to optimize the measurement process and processing of the sensor signal, are considered. The existing sensor arrays/e-nose systems for environmental monitoring are summarized, and future prospects and challenges encountered with metal oxide-based sensor arrays are highlighted.

Keywords: metal oxide sensors; chemoresistive detectors; environmental monitoring; sensitivity; selectivity; electronic nose



Citation: Tereshkov, M.; Dontsova, T.; Saruhan, B.; Krüger, S. Metal Oxide-Based Sensors for Ecological Monitoring: Progress and Perspectives. *Chemosensors* **2024**, *12*, 42. <https://doi.org/10.3390/chemosensors12030042>

Academic Editor: Elena Dilonardo

Received: 26 January 2024

Revised: 28 February 2024

Accepted: 2 March 2024

Published: 5 March 2024



Copyright: © 2024 by the authors. Licensee MDPI, Basel, Switzerland. This article is an open access article distributed under the terms and conditions of the Creative Commons Attribution (CC BY) license (<https://creativecommons.org/licenses/by/4.0/>).

1. Introduction

Monitoring of the environment is becoming an urgent need of our time, as its quality affects human and biota life. Industrialization, automobile exhausts, and the burning of fossil fuels are the most significant factors causing environmental pollution, including atmospheric pollution. This problem can be successfully solved with the help of gas sensors that rapidly and reliably detect a wide range of harmful gases in the ambient air environment. Among the different types of gas sensors, such as electrochemical, catalytic combustion, thermal conductivity, infrared absorption, and semiconductor metal oxide sensors (SMOs), the latter is the most common due to their high sensitivity, ease of manufacture, ultrasmall size, and cost effectiveness [1,2].

Research in the field of metal oxide gas sensors has developed rapidly in recent years. Thanks to the progress made in the miniaturization of chemical sensors, the latter can be integrated into low-cost small drones, which will exponentially increase the use of gas sensors for online environmental sensing. The versatility of the chemical sensor and drone combination will allow the rapid deployment of metal oxide-based sensors for gas monitoring, for example, in atmospheric research, industrial emissions detection, and environmental compliance control [3]. Also, metal oxide gas sensors are being widely investigated in the areas of healthcare, food safety and quality, and agriculture. In this case, e-nose systems are being developed to increase the sensitivity and selectivity of sensor devices [4–6].

There are a number of factors that affect the sensitivity, selectivity, and stability of a semiconductor metal oxide gas sensor, which can vary in each case. As a rule, dopants

improve the gas-sensing properties of SMOs by changing the microstructure or morphology, forming a stoichiometric solid solution, changing the activation energy, generating oxygen vacancies, or changing the electronic structure/band gap.

Different morphologies of metal oxides, such as 0D, 1D, and 2D [7], are used as sensing layers of gas sensors. The 0D morphology includes nanoparticles that are nanoscale in all three dimensions. At the same time, 1D and 2D particles are nanoscale in one and two dimensions, respectively. The inherent morphologies of 1D particles are wires, needles, whiskers, belts, rods, etc., while the 2D morphology includes metal oxide nanosheets.

Synthesis methods of metal oxides that allow the achievement of different particle morphologies include hydrothermal synthesis, the sol-gel method, thermal oxidation, electrolysis, electrospinning, chemical vapor deposition, and vapor-liquid-solid [8]. Varying the morphology during the wet-chemical synthesis of metal oxides is achieved by influencing the pH of the medium, temperature, addition of templates, etc. [9]. Depending on the process conditions, the CVD method can also produce different morphologies. For example, the work of [10] shows that by varying the precursor type, it is possible to obtain either 0D or 1D metal oxide particles, while the authors of [11] point out that the presence or absence of catalysts has a significant effect on the resulting morphology.

The morphology of the metal oxide (MOx) particles themselves such as nanowires, nanotubes, core-shell nanostructures, nanoneedles, nanosheets, and nanofibers contributes significantly to the sensing mechanism and thus to the performance of the gas sensor [12]. Therefore, recently, the research on chemical sensors based on one-dimensional (1D) semiconductor nanostructures of metal oxides with individual geometry has significantly intensified. Chemically sensitive 1D metal oxide nanostructures are usually considered resistors, whose conductivity changes during the charge transfer process, or field-effect transistors, whose properties are controlled by applying an appropriate potential to the gate. This suggests that 1D MOx nanostructures have significant potential for use in the next generation of chemical sensors that will be very small, low power, low cost, and more sensitive than existing commercial sensors [13,14].

The main issue in the usage of sensors based on metal oxide 1D nanostructures is ensuring the stable morphology of MOx particles, which directly affects the characteristics of the sensors. Many new strategies, in particular in-synthesis approaches, have been explored to solve this problem. For instance, nanomaterials synthesized by electrospinning have unprecedented advantages, including catalyst introduction, morphological control, thermodynamic stability, unique physicochemical properties, and composition control, and are attractive for the development of highly sensitive and selective gas sensors [15,16]. The formation of SMO-based nanoheterojunctions can effectively increase the response value of a sensing element due to the increased number of oxygen vacancies, active sites, and higher catalytic activity, resulting in a shorter detection time [17].

Despite the significant progress in the development of metal oxide-based gas sensors, their low selectivity and necessity to heat the sensing element for effective operation remain major problems. In this case, gas sensitivity can be improved by changing the particle size, nanoarchitecture, porous or hierarchical structure, doping or defect engineering, and design of nanocomposite and graphene hybrid sensor materials [18,19]. In turn, the development of gas sensors based on metal oxide nanostructures that operate at room temperature will reduce energy consumption, simplify device manufacturing, and improve the safety and stability of the sensors.

In terms of environmental monitoring, the most common gases to be detected are H₂, CO_x, NO_x, SO_x, and CH₄. Hydrogen is flammable over a very wide range of air concentrations (4–75%) and explosive over a wide range of concentrations (15–59%) at standard atmospheric temperatures [20]. Moreover, hydrogen produced by steam reforming of natural gas is not considered environmentally friendly [21].

CO_x causes the greenhouse effect, photochemical smog, and haze, threatening the urban atmosphere and human health [22]. CO is a colorless, odorless gas that is released during combustion. Outdoors, it contributes to air pollution, and indoors, inhaling large

amounts is very dangerous to human health, causing dizziness, confusion, loss of consciousness, and ultimately, death. A fairly large amount of CO₂ is emitted into the atmosphere as a result of burning fossil fuels, solid waste, and during the production of, for example, cement. Carbon dioxide in the atmosphere causes climate change by warming the planet but also affects the O₂ movement in blood.

Nitrogen oxides are the main greenhouse effect gases and harm the ozone layer. Thus, N₂O emissions lead to the destruction of the stratospheric ozone through nitrogen oxide-catalyzed processes [23]. The emission of NO_x (NO, NO₂, and N₂O) from vehicle exhaust and industry leads to nitrogen deposition, causing over-fertilization. Moreover, increased NO_x concentrations may result in respiratory and cardiovascular sickness in human beings.

SO₂ is produced due to the fossil fuel combustion and power generation process. It is a greenhouse gas and causes the greenhouse effect (atmospheric warming) [24]. In high concentrations, gaseous SO_x can harm trees and plants by damaging leaves and slowing growth. Sulfur dioxide and other sulfur oxides can contribute to acid rain, which can harm sensitive ecosystems. The long-term effect of SO₂ on human beings creates breathing problems, respiratory disorders, and visibility impairment [25].

CH₄ is a colorless, odorless, and flammable gas. It is also a potent greenhouse gas, which means it affects climate change by contributing to increased warming, according to the U.S. Environmental Protection Agency. Methane is released during coal, natural gas, and ore mining, at solid waste landfills, and on livestock farms [26].

Despite significant progress in the development of gas sensors based on metal oxides, achieving high rates of efficient gas detection is a very challenging task. Although they work effectively at high operating temperatures, the development of highly sensitive sensors capable of operating at ambient temperatures is essential to reduce power consumption. In general, it is believed that the development of low-temperature sensors should use materials with a high surface area, which is a combination of metal oxides with other metal oxides, either carbon or polymeric materials [27]. At the same time, the combination of modern equipment and the latest materials allows researchers to create new technological solutions incredibly quickly, which was the main reason for the creation of this work.

The purpose of this work is to highlight important advances in the field of metal oxide gas sensors, to distinguish important factors that complicate the development of gas sensors, and to review the development of old and new solutions to these problems. Particular attention is paid to the use of the latest developments in the context of environmental monitoring, which is becoming more relevant every year. We hope that this work will help to demonstrate the extent of the advances made in recent years, the current status of metal oxide gas sensors, and the main trends and direction of future development.

2. Environmental Monitoring by Metal Oxides Sensors

Semiconductor metal oxides have been widely used as the sensing layers of chemoresistive gas sensors for a variety of practical applications, with the main ones being real-time environmental monitoring, exhaled air diagnostics, and food freshness analysis. Nevertheless, chemoresistive metal oxide gas sensors have some disadvantages, such as low selectivity and high operating temperatures [28]. In order to overcome these disadvantages, metal oxide sensors are either decorated [29,30] or nanomaterials/nanocomposites are created [31,32]. In addition, chemoresistive metal oxide devices often suffer from nonlinear responses, signal fluctuations, and cross-sensitivity to different gases, which limits their use for air quality monitoring. To overcome these shortcomings, it has been proposed [33] to use the impedance method, which allows measuring dielectric excitation and provides sensors with a linear gas response, a wide dynamic range of gas detection, and high baseline stability, and also reduces the effect of humidity and ambient temperature on the output signal. The following are advances in metal oxide-based sensors for the environmental monitoring of gases such as H₂, CO_x, SO_x, NO_x, and CH₄.

2.1. H₂

Monitoring the presence of hydrogen in the air, which is generated during the steam reforming of natural gas, is an important task from the point of view of environmental protection. Furthermore, to ensure the safe use of renewable hydrogen energy sources, there is an urgent need to develop fast and sensitive sensors for leak detection.

For hydrogen detection, sensitive layers based on SnO₂, ZnO, TiO₂, Nb₂O₅, In₂O₃, FeO, Fe₂O₃, NiO, Ga₂O₃, Sb₂O₅, MoO₃, V₂O₅, and WO₃ have been investigated [34], among which SnO₂- and ZnO-based layers are the most promising. For instance, investigations into the morphology effect of SnO₂ and ZnO on sensitivity have demonstrated that nanobelts significantly outdo the other types of 1D nanostructures. Herewith, sensors based on ZnO are the most attractive due to their low cost, ease of preparation, and thermal/chemical stability [35,36].

In addition to variation in the morphology, the sensitivity of SnO₂ and ZnO to hydrogen can be increased by combining two metal oxides [34,37], creating composites with carbon materials [38], metal decorating [39], and creating core-shell nanoparticles [40]. For example, the researchers in [41] developed highly sensitive, stable, and selective sensors for gaseous hydrogen through the use of core-shell PdAu@ZnO nanoparticles and demonstrated that the core-shell sensors exhibit greater hydrogen sensitivity compared to pure ZnO.

Metal oxide sensors used for hydrogen detection mainly work as transducers that convert changes in physical or chemical properties into electrical signals. These sensors are classified into resistance-based, work function-based, optical, and acoustic sensors based on their detection mechanism [42].

Nanostructured thin-film sensors are generally used for hydrogen sensor fabrication due to their advantages, such as ease of implementation, good compatibility with integrated circuits, high sensitivity, and short response/recovery time. However, elevated working temperatures are still required for most thin-film sensors, which can lead to poor long-term stability and high power consumption [43].

To enhance gas selectivity and improve responses at lower temperatures, scientists have extensively studied the impact of grain size, porosity, orientation, surface doping, decorating, and device architecture on hydrogen sensor sensitivity. The selectivity problem is not as easy to solve because metal oxide semiconductor sensors cannot discriminate between H₂ and other combustible gases.

Research has demonstrated that hydrogen sensors employing single SMO 1D nanostructures can attain ultra-sensitivity, a fast response, high selectivity towards low concentrations of hydrogen, and long-term stability [43]. The metal oxide semiconductor sensing material must have high sensitivity, selectivity, and linear response. Sensitivity can be enhanced by surface functionalization, nanostructure engineering, or special signal processing. In addition, as more green hydrogen becomes available, the fabrication of hydrogen sensors with both acceptable sensitivity and fast responses at or near room temperature remains an important issue [44].

2.2. CO_x

Carbon oxide detection using a MO_x sensor is widely presented in the literature [45–47]. Most commonly, ZnO, SnO₂, and TiO₂ are discussed as key oxides for CO_x detection. However, sensitive materials based on CeO₂, In₂O₃, WO₃, CdO, CuO, composite oxides, and yttria-stabilized zirconia are also considered [48].

As the chemical inertness of CO₂ makes it difficult to detect, to date, only a few CO₂-sensitive materials have been found. Among these materials, various ZnO nanostructures showed high sensitivity. For example, sensitivity at the level of 0.1 ppm with an ultrafast response of <20 s is observed for zinc oxide nanoflakes [47]. Also, ZnO nanostructures obtained via hydrothermal synthesis have demonstrated responses in the range of 16–65% for CO_x detection at low temperatures [45].

For carbon monoxide, the situation is more predictable. In this case, various synthesis/manufacturing methods, including CVD, hydrothermal, screen printing, sputtering, spray pyrolysis, sol–gel, co-precipitation, electrospinning, the Peccini method, etc., are described along with their advantages and limitations [49,50]. Due to the alteration of the material's morphological and compositional characteristics, these methods allow the production of metal oxide-based films that are highly sensitive to CO. Thus, in the case of the CVD method, the sensitivity and other performance parameters can be enhanced due to the casting of surface conditions, pore/grain sizes, and morphology. The sensitivity of MO_x, synthesized via the hydrothermal method, depends mainly on the materials' structure and morphology, such as nanorods, nanoparticles, nanowires, nanosheets, nanotubes, and wall coatings. In spray and spray pyrolysis approaches, the sensitivity and other performance parameters can be improved due to the usage of alloying metals, in particular, Pd, Pt, Al, Cu, Au, Ga, and Co, among others [48].

Zhang et al. investigated the effect of the synthesis method, doping effect, and morphology on the performance of CO gas sensors based on the selected key oxides, such as ZnO, SnO₂, and TiO₂. For instance, authors have demonstrated that among ZnO materials, synthesized using various methods, powder obtained via the hydrothermal method has shown a 16.3% response to 0.8% CO₂ under UV light with a 19 s response time [51]. In turn, high sensitivity at low operating temperatures has been achieved for sensors based on SnO₂, synthesized via various synthesis methods, such as screen printing, solvothermal synthesis, sol–gel, the chemical method, sputtering, etc. [45].

Despite significant progress in the development of CO sensors, the issues of sensitivity, selectivity, low operating temperature, and low detection limit, as well as miniaturization, low price, etc., remain the major challenges to date. In order to obtain even more sensitive and selective CO_x sensors, researchers continue to work on improving the key operating parameters of gas sensing—the so-called 4S parameters—Sensitivity, Selectivity, Stability, and Speed. Finally, metal oxide-based sensors are expected to be in high demand for air quality monitoring in the near future. Flexible sensors are also expected to be integrated into smart devices for various applications.

2.3. SO_x

Available studies on sulfur dioxide detection also indicate the promising use of metal oxide nanostructures. For instance, the perspectives of NiO, NiO-modified metal oxide films, NiO-ZnO composites [52], and NiO-doped SnO₂ [53,54] have been explored for the manufacturing of effective gas sensors for toxic and dangerous gases. In their work, Chaitra et al. synthesized Al-doped ZnO thin films, which exhibited a sensor response of 71% towards SO₂ at concentrations below the threshold level value [55]. Tyagi et al. demonstrated that among different metal oxide catalysts (PdO, CuO, NiO, MgO, and V₂O₅) deposited on the SnO₂ surface, the SnO₂ film with NiO nanoclusters exhibited the maximum sensitivity of ~56 at a low operating temperature of 180 °C to 500 ppm SO₂ gas with a fast response time of 80 s [56]. The usage of NiO for SO₂ detection has also been proven to be promising in other studies [52,57,58].

However, currently, only electrochemical sensors are commercially available for the measurement of SO_x gases. The NASICON-based sensor is the most sensitive to this gas and also remains stable for a long time even in a highly corrosive atmosphere [25]. Therefore, the development of SO_x-sensitive metal oxide sensors remains an important task to be addressed in the near future.

2.4. NO_x

Numerous studies have shown the prospects of using SnO₂, WO₃, and ZnO metal oxides for NO_x gas detection [59–64]. For example, in [65], SnO₂ nanowires responded well to 5 ppm NO_x at a 200 °C operating temperature. One-dimensional ZnO particles modified with In₂O₃ showed response of 55 at a NO₂ concentration of 1 ppm, and a sufficiently high response (~18) was observed at a relatively low NO₂ concentration of 250 ppb [66].

Researchers are currently focusing on the development of low-temperature, stable, and highly selective NO_x sensors. The most extensive research is being conducted on the fabrication of ZnO-based nanocomposites and heterostructures [61,67]. The decoration of ZnO with precious metals such as gold, platinum, and others is also quite popular [68]. In addition, the influence of morphology, porosity, defects, and optical properties on the sensory properties of ZnO-based sensors are also being actively investigated [69].

In summary, NO_x sensors based on SnO_2 , WO_3 , and ZnO metal oxides have already demonstrated high sensitivity of up to 430% at room temperature [70–72] and can be easily embedded into instrumental platforms, for example, into the SOGS (Small Open General-purpose Sensor) platform. However, the reliability and sensitivity of ready-made sensor devices during real-time monitoring of the environment for several gases at the same time remain unresolved issues. In this sense, the main goal of further research should be related to ways to improve the reliability of sensor technology for measuring pollution in urban or field environments [73].

2.5. CH_4

The development of effective sensor materials with superior performance for the selective, fast, and sensitive detection of organic gases is important not only for environmental protection but also for human health. CH_4 can be successfully detected by various types of sensors, but MOx-based methane sensors are generally inexpensive, lightweight, reliable, durable, and poison-resistant. Nanocrystalline metal oxide CH_4 sensors are characterized by sufficient sensitivity; however, they have a number of inherent disadvantages, such as low selectivity, low and high operating temperature ranges, slow recovery, and significant dependence on temperature and humidity [74].

To increase CH_4 sensor selectivity, additional modification/doping of MOx nanostructures is required [75,76]. For instance, studies on the doping of metal oxides with precious and non-precious compounds exhibit the prospects of creating methane sensors based on ZnO thin films modified with non-precious metals, such as cobalt or Pn nanowires [77–79]. Also, researchers are proposing the use of metal-organic frameworks (MOFs) for the functionalization of metal oxides [80]. The latter have been widely investigated for their potential use as high-performance sensors for the detection of many different organic gases due to their large surface area, tunable pore size, functionalized sites, and interesting properties such as electrical conductivity, magnetism, ferroelectricity, luminescence, and chromism. The high porosity of MOFs allows them to interact closely with a variety of organic analytes, including CH_4 , resulting in easily measurable responses to various physical and chemical parameters.

The main problem with the detection of organic analytes in general and for CH_4 in particular is the simultaneous presence of multiple gases. A previous paper [81] proposes a new detection method based on ZnO metal oxide sensors that can selectively detect different types and concentrations of organic gases, including CH_4 . The method is based on signal processing under temperature modulation using a generalized regression neural network (GRNN).

2.6. Summary of Semiconductor Metal Oxide Gas Sensors to H_2 , CO_x , NO_x , SO_x , and CH_4 Gases

The performances of gas-sensitive properties of various SMO materials, along with particle morphology and the synthesis technique, are presented in Table 1.

Table 1. Gas-sensing performance of various SMO materials.

Target Gas/Concentration	SMO/Mode of Signal Transmission	Synthesis Technique/Particle Morphology	Sensor Parameters	Ref.
H ₂ 100 ppm	Pd ₃₅ Au ₆₅ @ZnO/ chemoresistive	Hydrothermal route/core-shell nanoparticles	Response: 80% Response/recovery time: 0.6/12 min Detection limit: N/A Operating temperature: 300 °C	[41]
H ₂ 400 ppm	SnO ₂ / chemoresistive	Hydrothermal/nanosheet-assembled nanoflowers	Response: 22 Response/recovery time: ~15/~17 s Detection limit: N/A Operating temperature: 350 °C	[82]
H ₂ 100 ppm	ZnO/ chemoresistive	Electrospinning, RF sputtering/ porous nanotubes	Response: 1.48 Response/recovery time: ~50/~200 s Detection limit: N/A Operating temperature: 200 °C	[83]
H ₂ 5 ppm	Au-decorated ZnO/ chemoresistive	Thermal CVD/ nano-network	Response: 21.5% Response/recovery time: 4/24 s Detection limit: N/A Operating temperature: 150 °C	[84]
H ₂ 250 ppm	Pt-Au@ZnO/ chemoresistive	Hydrothermal/bimetallic nanoparticles, nanorods	Response: 157.4 Response time: 115 s Detection limit: 50 ppm Operating temperature: 130 °C	[85]
H ₂ 40 ppm	PdO/WO ₃ nanohybrids/ chemoresistive	Hydrothermal/nanorods	Response: 8.02 Response/recovery time: 2.1/5.8 min Detection limit: 5 ppm Operating temperature: 200–250 °C	[86]
H ₂ 1000 ppm	Pd-decorated WO ₃ / chemoresistive	Magnetron sputtering method/films	Response: 586 Response/recovery time: 360/90 s Detection limit: N/A Operating temperature: 200 °C	[87]
H ₂ 20 ppm	Pd-decorated SnO ₂ / chemoresistive	Hydrothermal/nanosheets	Response: 75 Response/recovery time: 21/13 s Detection limit: N/A Operating temperature: 220 °C	[88]
H ₂ 50 ppm	PdO-decorated NiO/ chemoresistive	Ultrasonic spray pyrolysis/ needle-like thin films	Response: 82 Response/recovery time: 53/78 s Detection limit: 500 ppb Operating temperature: 250 °C	[89]
H ₂ 100 ppm	Pd@PdO/ γ-Fe ₂ O ₃ @GC Heterostructures/ chemoresistive	Solvothermal/core-shells, microcubes	Response: 96.2 Response/recovery time: 21/29 s Detection limit: 500 ppb Operating temperature: RT	[90]
CO 25 ppm	NiO-MOF/rGO/ chemoresistive	Hydrothermal method/nanoparticle aggregates	Response: 30 Response/recovery time: 30/70 s Detection limit: N/A Operating temperature: RT	[91]
CO 50 ppm	SnO ₂ -PdOx/ chemoresistive	Sol-gel method/nanoparticle aggregates	Response: 3.8 Response/recovery time: N/A Detection limit: 7.33 ppm Operating temperature: 500 °C	[92]

Table 1. Cont.

Target Gas/Concentration	SMO/Mode of Signal Transmission	Synthesis Technique/Particle Morphology	Sensor Parameters	Ref.
CO 300 ppm	SnO ₂ nanowires/ chemoresistive	Evaporation-condensation process, with vapor-liquid-solid growth mechanism/nanowires	Response: 1.8 Response/recovery time: 200/800 s Detection limit: N/A Operating temperature: 250 °C	[93]
CO 330 ppm	La _{0.8} Sr _{0.2} CoO ₃ / potentiometric	Radio frequency magnetron sputtering/thin films	Response: 15 Response/recovery time: 120/3000 s Detection limit: 10 ppm Operating temperature: 600 °C	[94]
CO 200 ppm	ZnO/SnSe ₂ / chemoresistive	Hydrothermal method/ rod-shaped, polyhedral nanostructures	Response: 14.8 Response/recovery time: 19/13 s Detection limit: 10 ppm Operating temperature: RT	[95]
CO 500 ppm	Pt-SnO ₂ / chemoresistive	Chemical oxidation in solution/nanoparticles	Response: 4.8 Response/recovery time: 1/3 min Detection limit: 50 ppm Operating temperature: 350 °C	[96]
CO ₂ 400 ppm	BaTiO ₃ -CuO/ chemoresistive	Plasma enhanced chemical vapor deposition/films	Response: 54 Response/recovery time: 30/230 min Detection limit: N/A Operating temperature: 300 °C	[97]
CO ₂ 1000 ppm	Ag doped ZnO/CuO nanoflowers/ chemoresistive	Hydrothermal Method/nanoflowers	Response: 18.4 Response/recovery time: 2.5–4.4/3.1–5.4 min Detection limit: 150 ppm Operating temperature: RT	[98]
CO ₂ 100 ppm	MoO ₃ nanorods/ chemoresistive	Vacuum thermal evaporation/nanorods	Response: 15 Response/recovery time: 8/40 s Detection limit: 50 ppm Operating temperature: 250 °C	[99]
CO ₂ 500 ppm	ZnO/CuO/RGO nanocomposite/ radio frequency identification	Hydrothermal method/nanorods	Response: 1.9 Response/recovery time: 19.1/32.5 s Detection limit: N/A Operating temperature: RT	[100]
NO ₂ 5 ppm	WS ₂ /SnO ₂ / optoelectronic	RT aqueous self-assembly/quantum dot-decorated nanosheets heterostructure	Response: 430% Response/recovery time: 10/9 s Detection limit: N/A Operating temperature: RT	[70]
NO _x 6 ppm	Au-decorated ZnO/ chemoresistive	Colloidal templating/1D nanorods	Response: 78% Response/recovery time: 110/100 s Detection limit: 550 ppb Operating temperature: RT	[71]
NO ₂ 1 ppm	ZnO/PbS nanocomposite/ chemoresistive	Hydrolysis/ nanorods	Response: 118–122% Response/recovery time: 3/4 min Detection limit: 26 ppb Operating temperature: RT	[72]

Table 1. Cont.

Target Gas/Concentration	SMO/Mode of Signal Transmission	Synthesis Technique/Particle Morphology	Sensor Parameters	Ref.
NO _x 10 ppm	In ₂ O ₃ / chemoresistive	Hydrothermal/mesoporous nanosheets	Response: 213 Response/recovery time: 4/9 s Detection limit: 10 ppb Operating temperature: 120 °C	[101]
NO ₂ 5 ppm	SnO ₂ / chemoresistive	Hydrothermal/ hollow nanospheres	Response: 5 Response/recovery time: 7/25 s Detection limit: 0.1 ppm Operating temperature: RT	[102]
NO ₂ 800 ppb	In ₂ O ₃ / chemoresistive	Hydrothermal/nanorods	Response: 14.9 Response/recovery time: 14/32 s Detection limit: N/A Operating temperature: RT	[103]
NO ₂ 10 ppm	rGO-CeO ₂ / chemoresistive	Solvothermal/nanosheets, nanocrystals	Response: 4.59 Response/recovery time: 100/258 s Detection limit: 0.3 ppm Operating temperature: RT	[104]
NO 50 ppm	In ₂ O ₃ / chemoresistive	Co-arc- discharge/nanoparticles	Response: 40 Response/recovery time: 10 s/4 min Detection limit: N/A Operating temperature: RT	[105]
NO ₂ 5 ppm	Ag-decorated ZnO/ chemoresistive	Modified polymer-network gel route/nanoparticles	Response: 1.545 Response/recovery time: 150/50 s Detection limit: <500 ppb Operating temperature: RT	[106]
NO 1000 ppm	Pt/SnO ₂ -WO ₃ / chemoresistive	Calcination method/nanoparticle aggregates	Response: 3.3 Response/recovery time: 40/206 s Detection limit: 10 ppm Operating temperature: RT	[107]
SO ₂ 5 ppm	LaNiTiO ₃ /potentiometric	Sol-gel method/nanoparticle aggregates	Response: 27.5 Response/recovery time: 40/206 s Detection limit: 0.05 ppm Operating temperature: 510 °C	[108]
SO ₂ 20 ppm	TiO ₂ /rGO nanocomposite/ chemoresistive	Calcination method/thin film	Response: 3.47 Response/recovery time: 456/134 s Detection limit: N/A Operating temperature: RT	[109]
SO ₂ 50 ppm	ZnO/ chemoresistive	Microwave-assisted hydrothermal/ nanorods	Response: ~100 Response/recovery time: N/A Detection limit: 5 ppm Operating temperature: 200 °C	[110]
SO ₂ 300 ppm	Sn-doped Al ₂ O ₃ / chemoresistive	The microwave irradiation method/nanoparticles	Response: 78.14 Response/recovery time: 17/200 s Detection limit: 10 ppm Operating temperature: 250 °C	[111]
SO ₂ 5 ppm	Cu-SnO ₂ / chemoresistive	Hydrothermal method/nanosheets	Response: 4 Response/recovery time: 14/17 s Detection limit: 1 ppm Operating temperature: 300 °C	[112]

Table 1. Cont.

Target Gas/Concentration	SMO/Mode of Signal Transmission	Synthesis Technique/Particle Morphology	Sensor Parameters	Ref.
SO ₂ 5 ppm	WO ₃ / chemoresistive	Hydrothermal method/ nanoparticles	Response: 50 Response/recovery time: 18/11 s Detection limit: 1 ppm Operating temperature: 260 °C	[113]
SO ₂ 20 ppm	γ-Fe ₂ O ₃ /surface acoustic wave	Chemical precipitation method/ nanorods	Response: 35 Response/recovery time: 65/65 s Detection limit: 2.5 ppm Operating temperature: RT	[114]
SO ₂ 10 ppm	Ni doped SnO ₂ / chemoresistive	Low temperature polyol route/ nanoparticles	Response: 6 Response/recovery time: 50/~2000 s Detection limit: 3 ppm Operating temperature: RT	[115]
SO ₂ 600 ppm	PVF/TiO ₂ / chemoresistive	Solution casting technique/ nanocomposites	Response: 83.75 Response/recovery time: 66/107 s Detection limit: 40 ppm Operating temperature: 150 °C	[116]
SO ₂ 15 ppm	SnO ₂ /MoS ₂ heterostructure/ chemoresistive	Hydrothermal method/ nanospheres	Response: 12 Response/recovery time: ~300/~600 s Detection limit: 1 ppm Operating temperature: RT	[117]
CH ₄ 100 ppm	Pd modified ZnO/ chemoresistive	Hydrothermal method/nanosheets	Response: 8.65 Response/recovery time: ~700/~250 s Detection limit: N/A Operating temperature: 200 °C	[79]
CH ₄ 1000 ppm	Pt-SnO ₂ / chemoresistive	Chemical oxidation in solution/ nanoparticles	Response: 65.6 Response/recovery time: 1/3 min Detection limit: 200 ppm Operating temperature: 350 °C	[96]
CH ₄ 5000 ppm	Ag-modified ZnO/ chemoresistive	Solvothermal route/flower-like microspheres	Response: 20.15 Response/recovery time: 118/119 s Detection limit: N/A Operating temperature: 200 °C	[118]
CH ₄ 1000 ppm	ZnO/g-C ₃ N ₄ composites/ chemoresistive	Precipitation-calcination route/ nanospheres	Response: 6.89 Response/recovery time: ~700/~300 s Detection limit: 500 ppm Operating temperature: RT	[119]
CH ₄ 60 ppm	TiO ₂ / chemoresistive	Hydrothermal method/ nanofibers	Response: 57 Response/recovery time: 99/162 s Detection limit: 5 ppm Operating temperature: RT	[120]
CH ₄ 1000 ppm	Pd/In ₂ O ₃ / chemoresistive	Hydrothermal method/ nanoflowers	Response: 1.16 Response/recovery time: 13/27 s Detection limit: N/A Operating temperature: 340 °C	[121]
CH ₄ 1000 ppm	NiO-modified In ₂ O ₃ / chemoresistive	Hydrothermal method/flower-like structure	Response: 1.3 Response/recovery time: 33/64 s Detection limit: N/A Operating temperature: 350 °C	[122]

Table 1. Cont.

Target Gas/Concentration	SMO/Mode of Signal Transmission	Synthesis Technique/Particle Morphology	Sensor Parameters	Ref.
CH ₄ 1000 ppm	TiO _{1.5} /ZnO/ chemoresistive	DC magnetron sputtering/ nanoparticles	Response: 1.2 Response/recovery time: 430/228 s Detection limit: N/A Operating temperature: 300 °C	[123]
CH ₄ 400 ppm	Pd-doped SnO ₂ / chemoresistive	Screen printing/ thick films	Response: 60 Response/recovery time: 8/73 s Detection limit: 50 ppm Operating temperature—350 °C	[124]
CH ₄ 50 ppm	V ₂ O ₅ / chemoresistive	DC magnetron sputtering technique/hierarchical nanostructures	Response: ~8 Response/recovery time: ~600/~550 s Detection limit: N/A Operating temperature: 100 °C	[125]

Analysis of the available literature shows that different variations of metal oxide compounds are employed to fabricate layers sensitive to H₂, CO_x, NO_x, SO_x, and CH₄ gases: from simple metal oxides to nanocomposites and/or heterostructures based on them. For instance, the decoration of metal oxide layers and the production of 1D and flower-like structures are popular techniques (Figure 1). The range of sensory properties of the metal oxide layers under consideration indicates that the final properties of the obtained selective layers rely on the structure, morphology, phase, and chemical composition of the metal oxides, which in turn can be alternated via the synthesis method and processing parameters. Numerous studies confirmed these observations [90,126,127]. The morphology and structure of SMO particles also have an impact on the electrical properties of metal oxide materials [113,128,129]. According to data presented in Table 1, the hydrothermal method is the most widely used synthesis method due to its simplicity and the potential to vary the particle morphology across a broad range. Nonetheless, other methods including sol–gel, CVD, electrospinning, and magnetron sputtering have also been extensively studied.

Sensor configuration is another significant aspect, which shall be considered for the development of high-performance sensing devices. Thus, in the case of NO detection at room and low temperatures, memristor-based sensors (Figure 1d) [130,131] appear to be the most promising candidates due to their miniature sizes, simple operation, low-cost manufacturing, and easy integration [132].

Furthermore, the data in Table 1 indicates that researchers primarily focus on identifying the aforementioned gases within the following concentration intervals: H₂: 5 to 100 ppm; CO_x: 25 to 1000 ppm; NO_x: 1 to 1000 ppm; SO_x: 5 to 600 ppm; CH₄: 50 to 5000 ppm. According to the literature, feasible responses for these gases of 586, 54, 430, 100, and 65.6, respectively, have been achieved so far. Regrettably, the selectivity of metal oxide sensors is not often considered by scientists, remaining mostly understudied. However, the information available in the literature shows a wide range of selectivity values depending on the nature of associated gases. For instance, the selectivity of hydrogen sensors ranges from 1.3–156 [85], carbon monoxide sensors from 25–37 [92], and methane sensors from 6.3–68 [79,96]. The variation in metal oxide morphologies, doping, and the creation of heterostructures allowed a reduction in response/recovery time of 10–20 s. Moreover, it can be noted that there is a trend towards gas sensors operating at room temperature, which implies researchers' efforts to minimize energy consumption and reduce costs. This indicates that researchers are increasingly making progress in creating highly sensitive, selective, miniaturized, and energy-efficient sensors based on metal oxides. Thus, to date, metal oxide sensors have demonstrated sufficiently high responses, sensitivity, and repeatability at room temperature. However, some challenges remain in their development. These often include low selectivity, insufficient lifetime, and problems in creating optimal geometric

characteristics of the sensors [31]. Overcoming these shortcomings requires additional in-depth theoretical (e.g., DFT modeling) and experimental studies, as well as the use of modern micro-industrial approaches (e.g., 3D printing) to create the desired design and reduce the time for sensor fabrication.

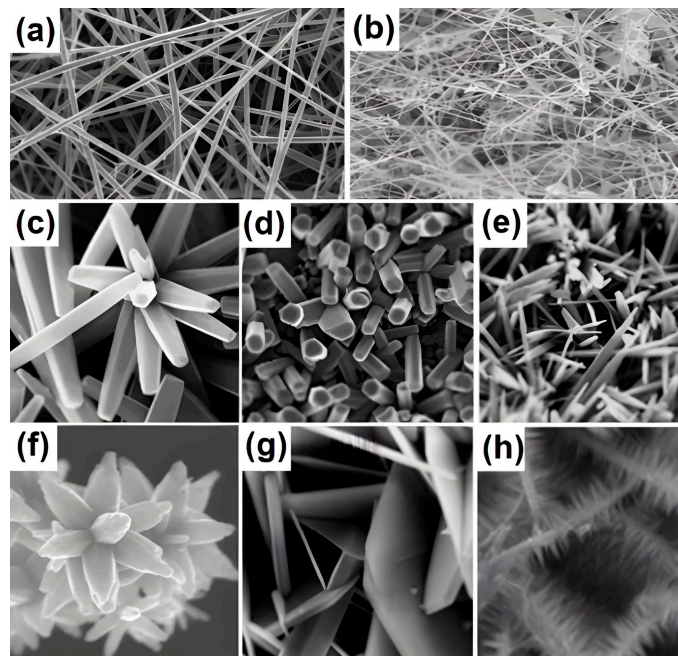


Figure 1. Typical nanostructures of metal oxides: (a,b) 1D structures. Reprinted with permission from [131]. Copyright Creative Common CC BY license. (c–h) flower-like structures. Reprinted with permission from [130]. Copyright Creative Common CC BY license.

3. Multisensor Systems/e-Nose Based on Metal Oxides for Environmental Monitoring

Most commercial gas analyzers have a wide range for the detection of gases but usually employ different sensor types (metal oxide, electrochemical, optical, thermal, etc.) in one device, which leads to increased costs, bulky systems, and reduced life span. According to the data presented in Section 2, metal oxides are promising materials for creating affordable sensors based on them; however, they suffer from insufficient sensitivity and selectivity. The low-selectivity problem of SMO gas sensors can be solved by creating so-called e-nose devices. Such systems are based on sensor arrays, which do not exhibit high selectivity but rather require special statistical data processing, as well as the creation of gas signature databases, which also leads to an increase in the costs and a narrowing of their application scope [22,133]. The e-nose system overcomes the limitations of single SMO gas sensors by collecting response patterns of the gas sensors in different conditions with different driving temperature parameters [133].

Considering the fact that most air pollution has a complex composition, such multisensory systems are essential for environmental monitoring. For instance, CO_x , hydrocarbons, and suspended particles are the main components in automobile exhausts [22]. CO_x , NO_x , and SO_x are emitted from combustion processes of coal, oil, and waste plants. Nitrogen oxide can be attributed to fertilizer production. NO_x and CH_4 are released by the digestive processes in livestock waste management. Besides human activities, natural disasters are other sources of air pollution. Thus, CO and NO_x gasses are formed during wildfires, and volcanic eruptions cause emissions of nitrogen compounds and SO_2 [134]. In the area of environmental monitoring, e-nose systems can replace traditional analytical methods, providing real-time detection instead of costly analysis tools that often require long processing time [135]. For instance, in contradistinction to the determination of odor concentrations in gas samples by dynamic olfactometry [136], electronic noses can be used for continuous

air monitoring and are able not only to measure the gas concentration but also to provide information regarding odor type [135].

Some relevant parameters for the development of gas monitoring systems for environmental applications are listed in Table 2. Furthermore, the greatest attention should be paid to the set of characteristics, such as simplicity, rapidity, robustness, reliability, and sensitivity [137].

Table 2. Requirements for environmental gas-monitoring systems [137].

Parameter/Specificity	Example
Application type	Qualitative/Quantitative analysis
Measurement type	Continuous/Discrete
Device location	In situ/Remote
Environmental	Controlled/Variable, Harsh/Normal
Power	Autonomous/Mains

To date, multiple research studies have been conducted on the detection of gas compositions using sensor arrays. Betty et al. demonstrated the real-time detection of NH_3 , H_2S , and NO_2 gases at room temperature using a SnO_2 nanocrystalline thin film. The developed sensor showed not only sufficient selectivity to the detected gasses in the presence of other interfering gasses but also high reliability with no changes in the response at high humidity up to 98% [138]. In their work, Kang et al. confirmed the significance of deep learning algorithms for the precise pattern recognition of sensor responses. The authors fabricated a sensor array based on SnO_2 , In_2O_3 , WO_3 , and CuO nanocolumnar films for real-time selective CO , NH_3 , NO_2 , CH_4 , and $\text{C}_3\text{H}_6\text{O}$ detection. The obtained sensor responses of the gas sensor array to the target gasses overlapped in the specific concentration ranges. In turn, it was possible to perform pattern recognition of the sensor signals by employing a convolutional neural network with a learning algorithm matrix (Figure 2). As a result, a high accuracy of 98% for gas classification with a very short response time was achieved. In addition, the authors confirmed the possibility of simultaneous gas concentration predictions with an average error of 10% [133].

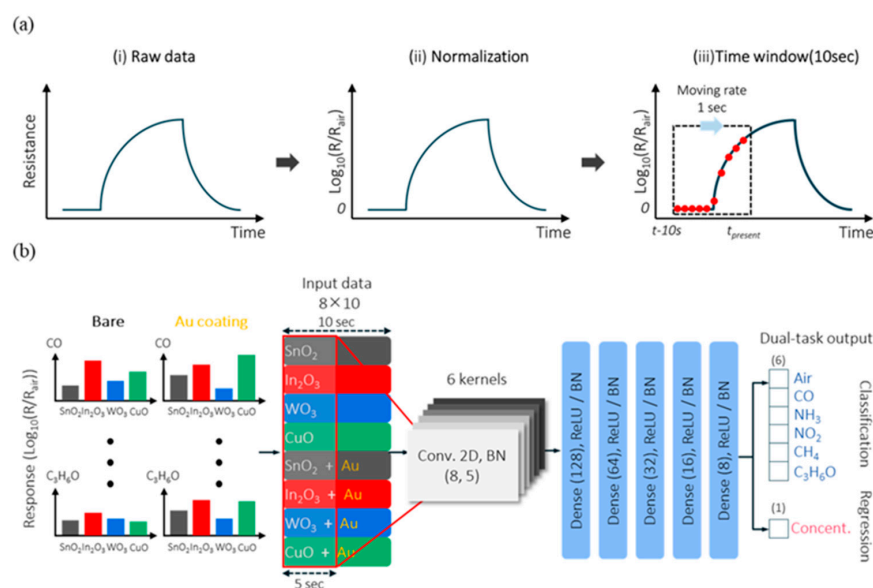


Figure 2. (a) Schematic illustration of the sensing data preprocessing; (b) structure of the convolutional neural network for gas species recognition. Reprinted with permission from [133]. Copyright © 2022, American Chemical Society.

In general, multisensor systems are promising devices for air quality assessment, gas detection, the quantification of specific compounds, and control processes at lower costs. However, for real-time continuous environmental monitoring, specifically developed and fine-tuned e-nose devices able to produce accurate and reliable results are required. Simple instruments for the detection of gas leakage and the evaluation of gas concentration are not suitable for these purposes [135]. The challenges of e-nose usage in the field of environmental monitoring are mostly related to the adjustment of process parameters for outdoor applications due to the instability of the sensor signal with variations in temperature and humidity [139,140], cross-sensitivity to interfering substances [141], and the problem of sensor response drift over time [142–144]. On the other hand, sensor array systems are able to provide reliable results with high accuracy when the temperature and humidity are kept at constant values [139], and the same is related to the presence of other interfering gases [141]. The problem of sensor drift over time significantly affects the device's reliability. Thus, an investigation of sensor array performance in a long-term period after sensor calibration demonstrated a radical deterioration of gas recognition over time from 98% to 20% after 3 years [145]. To avoid sensor drift over time, periodic re-calibration, as well as the use of specific software or specific equipment, is proposed [146,147].

4. Configuration and Geometry of Metal Oxide Sensors

The typical architecture of metal oxide-based gas sensors is generally represented by a sensitive layer deposited on the substrate with electrodes. Electrodes are one of the main elements of sensor construction and are used for the readout of the conductivity change in the sensing surface layer depending on the presence of gas in the environment. To date, several configurations of the electrodes of MOx sensors, such as cylindrical, disk-type, interdigitated, and memristor-type, have been proposed (Figure 3). In *cylindrical* gas sensors, the electrodes are deposited on or wound up around the cylindrical alumina substrate and covered with a layer of sensitive material (Figure 3a) [148,149]. To produce *disk-type* electrodes, the sensing material is sintered in pellet form and then the electrodes are deposited on both sides of the pellet (Figure 3b) [148–150]. Two-finger electrodes that comb parallel to each other with a fixed space between them form the *interdigitated* (IDE) sensor configuration pellet (Figure 3c) [148]. In the *memristor type* or so-called top–bottom (TBE) sensors, the sensing metal oxide material is sandwiched between the top and bottom electrodes (Figure 3d) [151].

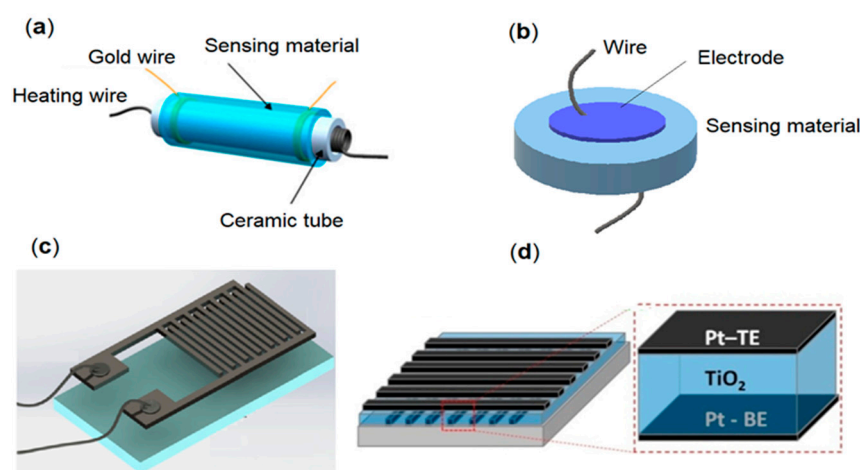


Figure 3. Configurations of the electrodes used in metal oxide-based gas sensors: (a) Cylindrical. Reprinted with permission from [152]. Copyright Creative Common CC BY license; (b) disk-type; (c) interdigitated; Reprinted with permission from [16]. Copyright Creative Commons Attribution 4.0 International License; (d) memristor-type. Reprinted with permission from [153]. Copyright © 2017 Elsevier B.V.

The interdigitated and memristor-type sensors are the most widely accepted electrode configurations of metal oxide-based gas sensors. IDE has an easy-to-produce stable geometry, which ensures a large active area between the electrodes, resulting in enhanced electron conduction and reduced resistance of the sensitive film [148,154,155]. To fabricate an interdigitated sensor, IDE electrodes are deposited onto the desired substrate (Si, glass, or Al_2O_3) using the microfabrication process, such as patterning and lift-off, and then the sensing material is coated on the top of electrodes [149]. The deposition of the sensing material on already-fabricated electrodes allows one to avoid any damage to the sensitive layer [150]. In the TBE geometry, one of the significant advantages is the equally small thickness of the sensitive film and lower distance between the electrodes (below 2 μm to as low as 40 nm) [156]. The thickness of the MOx layer of only several tens of nanometers can be achieved even without using sophisticated lithography methods, which in turn results in a very small interelectrode distance and, therefore, a high electric field even at small voltages [157]. Furthermore, the size of memristor-based sensors ranges from the nano- to micro-scale, while a typical gas sensor is usually a few micrometers in size [132].

As the gas-sensing characteristics depend strongly on electrode spacing, including the width of the digits and spacing between digits [148,158], an improvement in sensor performance can be achieved by altering the electrodes' geometry. For instance, a change in the electrode gap size influences the resistance value, and consequently, the sensitivity. A better gas sensor response is achieved when the spacing between electrodes is less than the electrode's width [159]. This is explained by the increased current conductivity of the sensing film for the closed electrode spacing due to the short path for current conduction. The wide gap between electrodes in turn results in current flow in both horizontal and vertical directions, thereby sampling a wider area [150]. However, the choice of the electrode gap size may also depend on the gas concentration. In their work, Shaalan et al. investigated the effect of electrode spacing on NO_2 gas-sensing properties and concluded that higher sensitivity to lower NO_2 concentrations was obtained for the short gap size of 1 μm . On the other hand, the authors observed that sensors with larger electrode gaps (30 μm) became highly sensitive to high NO_2 concentrations [160]. A study of the effect of micro-gap electrodes with gap sizes in the range of 0.1–1.5 μm on sensing performance demonstrated that the sensitivity to diluted NO_2 was almost unchanged for gap sizes larger than 0.8 μm but increased significantly with the decreasing gap size. The enhanced sensing behavior for the smallest gap size of electrodes is explained by the resistance change at two boundary types—the grain boundary and the electrode–grain interface [161].

Nguyen Minh et al. designed nanogap IDE electrodes for gas-sensing applications with controllable gaps in the range of 50–250 nm (Figure 4) and demonstrated that decreasing the IDE's gap from the micro- to nano-range leads to an improvement in sensitivity of up to 35 times. The authors confirmed that the developed nanogap IDE can be used for the detection of very small analyte amounts (as low as 6 ppm) and sensitivity could be further enhanced by increasing the electrode area [162].

Similar to electrode spacing, electrode width contributes significantly to the electrode–grain interface, and as a result, affects the sensitivity of gas sensors. Miyaji et al. investigated the sensitivity of WO_3 microsensors with different electrode widths (10 and 50 μm) to NO_2 and found that the sensitivity values were 2–3 times higher for the sensor with a 50 μm electrode width compared to the 10 μm sensor [163].

Besides the electrode spacing and electrode width, the electrode position can also contribute to the response of gas sensors. It has been assumed that the deposition of the sensitive layer above the electrode provides a larger surface area for interaction with gas molecules [154]. Nevertheless, the research work of Prajesh et al. on the positioning of interdigitated electrodes with respect to the sensing layer demonstrated that the sensor shows a significantly higher response to ammonia when the electrodes are placed above the sensing film (45% sensor response with top placement of electrodes in contrast to 25% sensor response for bottom electrode positioning). In this case, the enhanced gas sensor

response is related to the fact that the majority of reactions between the gas and the sensing film, therefore the top electrode provides a more accurate reading of the resistance changes compared to bottom-placed electrodes. The electrode position becomes even more notable when the thickness of the sensing film is higher than 100 nm since, in this case, the overall sensor response is highly dependent on the surface changes [164].

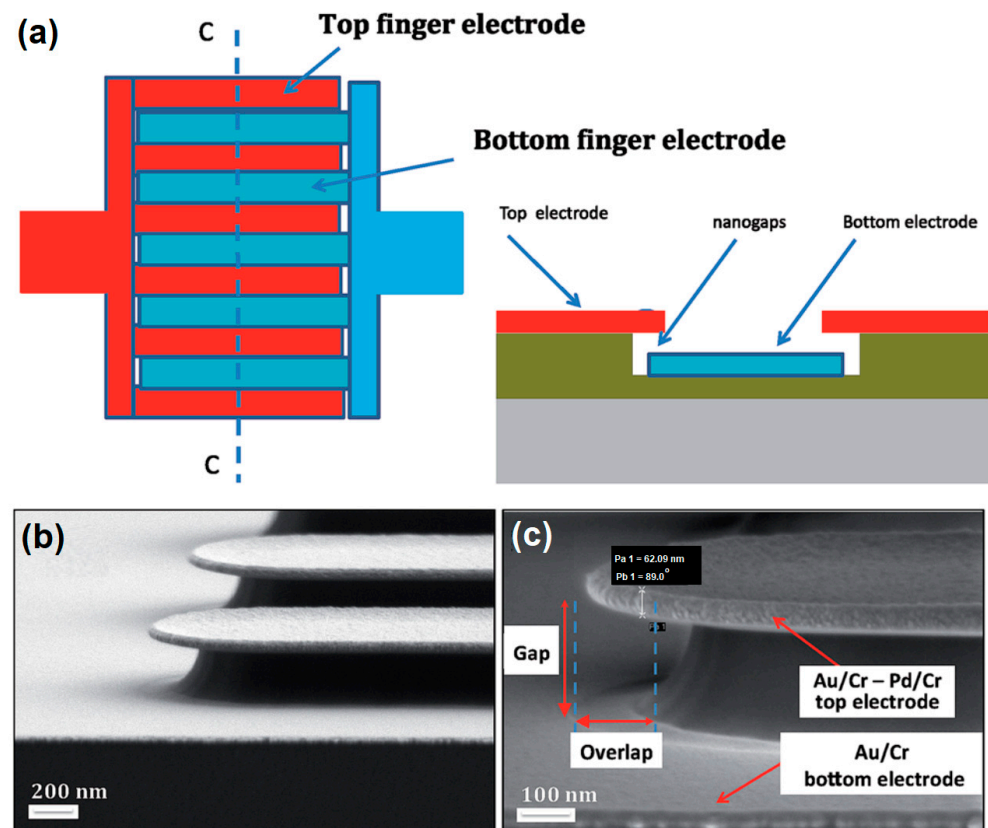


Figure 4. Interdigitated nanogap electrodes: (a) Overview and cross-section; (b,c) SEM images of the bottom and top electrodes. Reprinted with permission from [162]. Copyright © CC BY 3.0.

In this manner, interdigital and top–bottom electrode designs with controlled electrode widths and electrode gaps in the nano-range are the preferable sensor configurations to obtain high-sensitivity semiconductor metal oxide sensors. The variation in sensor geometry influences the active area of the sensitive film, leading to the enhancement of electron conduction and a reduction in resistance values, which in turn plays a major role in sensitivity improvement.

5. Detection Mechanism and Parameters Affecting the Sensitivity/Selectivity of the Sensors

5.1. Detection Models of Gas-Sensing Processes

Gas-sensing mechanisms for semiconductor metal oxide sensors have been extensively studied and are generally well-understood. For SMO sensors, the interaction between gas molecules and the surface and/or bulk of the oxide leads to a change in its electrical properties, which can be registered and interpreted by appropriate measuring equipment. The most commonly referred to theories are the electron depletion layer (EDL) theory and the hole accumulation layer (HAL) theory, which describes microscopic changes in the material itself, as well as the bulk resistance control mechanism and the gas diffusion control mechanism, which describe the physical and chemical interactions between the gas

and the sensing material [165]. These theories and mechanisms are often related and used in combination for better modeling of the gas-sensing process.

The **oxygen adsorption model** is one of the most common models used to describe gas-sensing processes for both n-type and p-type SMOs. This model suggests that the gas-sensing properties of the SMO originate from the presence of point defects—oxygen vacancies on the surface of the oxide, which eventually adsorb atmospheric oxygen to form negative O_2^- , O^- , and O^{2-} ions, taking electrons from the conduction band. This process leads to the formation of a depletion zone near the surface and an increase in the potential barrier at the oxide grain boundary. As a result of these phenomena, the oxide surface behaves like an n-doped semiconductor, especially at high temperatures [166]. The interaction with a reducing gas leads to a reduction-oxidation reaction with sorbed oxygen anions, returning electrons to the conductivity band, shrinking the depletion zone, and restoring electrical conductivity. Interaction with an oxidizing gas typically results in a further decrease in conductivity. In p-type semiconductors, due to the metal-ion-deficient defects, hole charge carriers are predominant. The hole accumulation zone is present, which grows with the adsorption of molecular oxygen and the formation of oxygen anions, leading to a decrease in electrical resistance. Interaction with the oxidizing gas leads to a reduction in oxygen anions, its replacement by oxidizing gas atoms, enlargement of the hole accumulation zone, and a further decrease in electrical resistance. Conversely, exposure to a reducing gas narrows the hole accumulation zone and causes an increase in electrical resistance [147].

In the case of the memristor-type sensors, the non-stoichiometry of the sensitive layer plays an important role in the generation of oxygen vacancies, thus affecting the overall sensing mechanism. Haidry et al. demonstrated that annealing of the Pt/TiO₂/Pt sensor structure results in the formation of two different zones in the sensitive layer: TiO₂ composition near stoichiometry and non-stoichiometric TiO_{2-x} at the bottom electrode. In turn, the thickness of the non-stoichiometric TiO_{2-x} zone plays a dominant role in the sensing mechanism and may result in higher sensitivity due to the changes in the depletion layer [153].

Another phenomenon that must be taken into account when considering the mechanisms of gas sensitivity is **chemical absorption/desorption** itself. This process usually has a small but measurable effect on the sensor response. The chemical adsorption of gases on the surface of the oxide can lead to the formation of new compounds with different electrical properties, which will affect the electrical conductivity of the sensor material, such as the formation of SnS₂ on the surface of SnO₂ when sensing H₂S gas [167]. In addition, chemisorption can, in some cases, improve the sensitivity of the sensor in a vacuum or inert atmosphere, as the gas can be adsorbed directly to oxygen vacancies, as described in [168] for certain concentrations of Cl₂ gas. In [82], the improved response of the SnO₂ sensor to H₂ in a vacuum is also demonstrated, which was attributed to the chemical adsorption of hydrogen and the subsequent shift in the valence band.

5.2. Parameters Affecting Sensor's Performance

Surface morphology and particle size naturally affect the sensitive characteristics of SMOs. Given the crystalline nature of metal oxides, they can form a variety of micro- and nanostructures of different dimensions, densities, and geometries, dramatically changing their electrical characteristics and interaction with different gases [169,170]. At a more basic level, it is known that reducing the size of oxide particles can improve the sensing properties of the sensor by increasing the specific surface area and reducing the surface charge density [10,171]. With a sufficiently small particle size (less than two Debye lengths), the electron depletion zone or hole accumulation zone extends over the entire thickness of the oxide particle, resulting in the strongest response [166]. Considering the processes described in the oxygen adsorption model, a high surface-area-to-volume ratio and the presence of exposed planes with crystal defects improve the sensing characteristics of metal oxides. The type of the exposed crystal facet directly affects the rate of chemisorption and electron

transfer processes [82,166,172]. Changing the surface morphology can not only alter the sensitivity of the sensor to a particular gas [83,101,173,174] but also enables the sensitivity of the same material to different gases—in [175], the change in the sensitivity mechanism depending on the surface morphology and the resulting detection of H₂S and NO₂ using dispersed nanoparticles and SnO₂ clusters is demonstrated. For instance, previous authors have shown that a SnO₂ small nanoparticle film (Figure 5a) has more efficient contact with plenty of conducting channels, leading to a larger current enhancement signal. In the case of the SnO₂ big cluster film (Figure 5b), fewer conducting channels among clusters result in a limited sensing signal. However, the morphology effect is strongly dependent on the gas nature. Thus, the SnO₂ big cluster demonstrated better sensitivity towards NO₂ down to ppb concentrations [169]. Xu et al. demonstrated control over the number of oxygen vacancies on the surface of CeO₂ nanowires by controlling the composition of the atmosphere during annealing [176]. With the help of precise control over the synthesis conditions and modern approaches, such as refined GO and rGO synthesis and modification procedures [177], and extensive use of organic precursors [178,179], it is possible to obtain quite complex and exotic structures with defined morphologies. An example of this is the CuO-ZnO cubic nanostructures with excellent sensitivity to acetone and a detection limit of 9 ppb: such a structure promotes the formation of a large number of p-n heterojunctions, which improves the sensor's performance [179]. In [180], the authors developed a method for the controlled synthesis of hollow GaFeO₃ microcubes, which allows modulation of the size and microstructure of such micro-assemblies. Tests conducted with this sensor with such a morphology have shown an optimum response of 7.4 for 200 ppm of triethylamine with a 9 s response time at 200 °C.

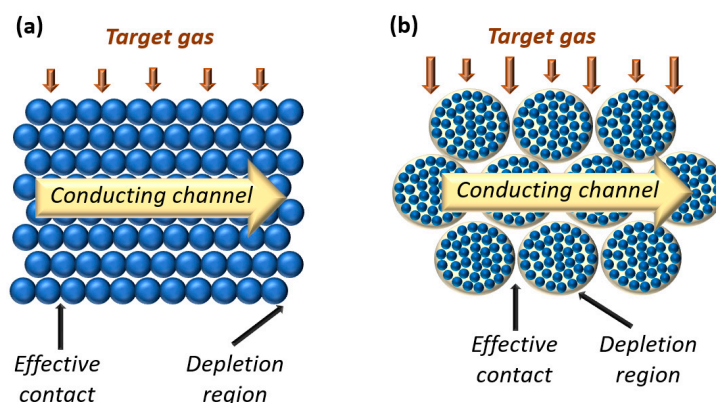


Figure 5. Schematic of SnO₂ films of different morphologies: (a) small nanoparticles film; (b) big cluster film. Adopted from [175].

Operating temperature is one of the key factors that directly affect the performance of metal oxide sensors. For the majority of metal oxides, the normal operating temperature is in the range of 150–500 °C, but depending on the type of oxide, surface morphology, and target gas, it can be as low as room temperature or as high as 1100 °C [12,181–183]. The process of chemisorption of oxygen and the formation of negative ions at a sufficient rate usually occurs at higher temperatures [12,165], which, as mentioned above, is one of the key elements of the gas-sensing process. In terms of chemical kinetics, an elevated temperature accelerates the reactions that occur on the surface of the oxide [184]. The variety of effects that the operating temperature has on SMO opens up interesting opportunities for gas sensors. Particularly, at different temperatures, the response and sensing range of the sensor can change as observed in [168], where, at temperatures of 300–400 °C, a WO₃ nanowire sensor demonstrated a decrease in response with an increase in the Cl₂ gas concentration; at temperatures of 250 °C or lower, such a behavior was no longer observed. Alternative sensitivities can occur at different temperatures, as shown in [185], where a CuO thin-film sensor exposed to different VOCs demonstrated an enhanced response to

2-propanol at 225 °C, while at 250 °C, the response to ethanol was significantly higher. Even the changes at an ambient temperature in combination with humidity variations can lead to false predictions of the gas source location when employing gas distribution mapping algorithms [186]. The response speed can be altered significantly with the change in operating temperature; a SnO₂/rGO sensor in [187] demonstrated a decrease in response time from ~400 s to almost ~200 s and faster recovery with an increase in the working temperature from 200 °C to 250 °C. Taking advantage of the known patterns of temperature effects on metal oxides, Yuan et al. achieved the detection of various VOC components using a single ZnO sensor using temperature modulation and a general regression neural network (GRNN) statistical model [81].

One of the important challenges constantly being faced by researchers is the efficient operation of sensors at room temperature without sacrificing sensor performance. Room temperature operation greatly expands the possible use of metal oxide sensors for wearable and medical applications, in explosive atmospheres, and in low-power applications. In recent years, much effort has been invested into solving this problem, opening up many new possibilities. Particular attention has been given to photoactivated metal oxide sensors: the use of UV radiation can improve the response and recovery time of sensors based on unmodified ZnO, SnO₂, and In₂O₃ at RT [84,102,103,188]. The change in the sensing properties of SMO sensors in the presence of UV radiation is usually associated with optoelectric and photocatalytic processes that can occur on the surface of the oxide. UV radiation that has energies higher than that of the band gap of the metal oxide causes the generation of electron–hole pairs in the sensing material that ultimately increases the number of reactive adsorbed oxygen species [18,189]. Photoactivation with UV radiation also intensifies adsorption/desorption processes [105] and may cause photocatalytic processes to occur on the surface of metal oxide [76]. In [190], a polyaniline/NiO-loaded TiO₂ sensor utilizing UV radiation showed high sensitivity to acetone (a minimum concentration of 176.2 ppb) and excellent stability at RT. The authors of [70] demonstrated the use of WS₂/SnO₂ 2D/0D heterostructures with UV activation to achieve an improved NO₂ response and fast response/recovery. Reduced graphene oxide and CeO₂ (rGO-CeO₂) heterostructures have demonstrated improved NO₂ sensitivity and response/recovery time at RT in the presence of UV radiation [104]. Numerous methods have also been developed to improve the performance of SMO sensors at room temperature without photoactivation. Pedowitz et al. proposed a δ-MnO₂/epitaxial graphene/silicon carbide heterostructure that demonstrates selective sensitivity to NO₂ and NH₃ at room temperature [191]. The use of rGO fibers coated with MoS_xSe_{2-x} with an increased Se content in [192] allowed the rapid recovery of the sensor surface with no additional heating. In [31], the authors exhaustively covered the latest advances in the use of hybrid polymer–metal oxide mixtures as gas sensors operating at RT. The use of bimetallic Pt–Au particles on ZnO nanorods, as demonstrated in [85], allows one to achieve a sensitivity of up to 250 ppm H₂ with fairly high selectivity. Decoration with noble metals typically improves the sensing properties of SMOs by increasing the sensitivity and response speed to certain gases (H₂, NO, NO₂, H₂S, and CO), as discussed in detail in [29].

Humidity is one of the factors that affect the sensitivity and selectivity of metal oxide sensors in real-world applications. In low-humidity conditions, water molecules are chemically adsorbed at active sites on semiconductor metal oxide surfaces, resulting in the formation of hydroxyl groups and mobile protons. At high humidity levels, all active sites are occupied by the previously chemisorbed water molecules, leading to the formation of physically adsorbed layers on top of the chemisorbed layer. This results in the formation of hydronium ions (H₃O⁺), and electrical conductance occurs due to proton H⁺ hopping between neighboring water molecules. Higher humidity levels also lead to a reduction in chemisorbed oxygen anions and target gas adsorption due to competition with water molecules [193]. This typically leads to reduced sensitivity and baseline resistance drift [194]. Various strategies can be employed to negate the impact of humidity on SMO sensors. Utilizing higher operation temperatures of up to 450 °C leads to the removal

of hydroxyl ions from the sensor surface, resulting in a full signal recovery in several minutes [181]. Nair et al. demonstrated that the formation of ZnO@MOF heterostructures is promising for a reduction in humidity cross-sensitivity. In this case, the ZnO/MOF interface acts as a diffusion barrier, resulting in the “trapping” of water molecules [195]. The formation of solid stoichiometric solutions of different oxides, for instance, Sn/Ti or Sn/Ti/Nb, was found to decrease the cross-sensitivity to humidity due to the lowering of the interaction strength with water by surface modification [196]. Abdullah et al. proposed a mathematical correction model to predict the corrected sensor response regardless of humidity changes throughout the experiment. The developed model allowed them to obtain more uniform sensor performances for more stable and reliable gas-sensing operations [194].

5.3. Methods of Processing Sensor Signals to Improve Sensitivity/Selectivity of the Sensors

With the development of SMO sensor technologies, requirements for sensor performance and efficiency have gradually increased, and new applications and tasks have emerged. A logical consequence of recent advances in microelectronics, algorithms, statistics, and artificial intelligence is the integration of these technologies into the field of SMO sensors. New ways to improve sensor performance have been discovered, which now include not only modifying the sensor structure or its chemical composition but also optimizing the measurement process and processing of the sensor output. The classical method of measuring the response of a metal oxide sensor is the measurement of resistance change [182], but measuring changes in complex resistance [197], capacitance [198,199], and measurements under alternating current conditions [200] allows us to enhance and optimize the efficiency of sensors from multiple angles. This amount of data that can be measured in real time requires adequate processing for its effective interpretation. Modern equipment allows us to achieve such goals while offering low power consumption and a compact form factor. The development of an integrated system consisting of a high-electron-mobility transistor (HEMT) H₂ sensor and a readout-integrated circuit is described in detail in [201]. HEMT's performance typically suffers from process, temperature, and voltage variations during the manufacturing process, which affects the repeatability of measurements and limits their application. The proposed readout circuit can be integrated with the sensor on the same chip and implements mechanisms of sensitivity nonlinearity correction, noise suppression, and calibration at the hardware level with a power consumption of only 3.1 mW and a resolution of 1 ppm. Another paper [202] demonstrated the use of a Kalman filter and absolute-deadband sampling to process signals from four different commercial gas sensors and determine the direction of the isopropyl alcohol “odor” source. These processing techniques allow us to compensate for the relatively slow response and recovery times of SMO sensors and detect quick changes in target gas concentrations. In [203], Burgués et al. utilized similar algorithms, a quadcopter, and two commercial SMO sensors to detect ethanol vapor sources in closed rooms and created a 3D map of gas concentration with a special resolution of 1.38 m. Notably, the measurements were conducted during continuous “sweeps” across the rooms, demonstrating the ability of the proposed algorithm to be utilized effectively and interpret data from relatively slow SMO sensors. The authors of [110] demonstrated the ability to effectively detect and distinguish between three different gases (O₂, SO₂, and NO₂) in a mixture with a single ZnO-based sensor. To achieve this functionality with an error of under 2%, resistance and impedance measurements were used, followed by data processing by an artificial neural network. Another previous paper [204] showed the use of conventional machine learning algorithms (random forest, naïve Bayes, support vector machine, and multilayer perceptron) to prepare a dataset of various gas concentrations and interpret data from a single SnO₂ sensor, which made it possible to distinguish formaldehyde, 2-propanol, toluene, and methanol and estimate their concentrations.

However, the application of specific signal-processing approaches, for instance, machine learning algorithms and artificial neural networks, also introduces certain limitations

and challenges specific to these technologies. The utilization of artificial intelligence processing introduces additional inaccuracies due to the inherently imprecise nature of AI algorithms. The application of even relatively basic machine learning techniques also adds to the issues of algorithmic bias and the quality of the initial dataset used to train the algorithm [205]. The initial dataset, known as the training dataset, generally comprises various parameters including electrical conductivity, impedance, and relative humidity for various concentrations of the target gas or a mixture of gases [159]. Calibrating metal oxide sensors to account for physical variations in individual samples can be significantly more difficult when using complex data processing algorithms and may require a new training dataset [160,206]. These factors increase the complexity and hinder the use of these technologies in cases where high reliability and confidence in the accuracy of the data are required [205].

Despite these challenges, such technologies offer a new angle on improving the performance of gas sensors. Clever use of the effects of nonlinearity and cross-selectivity, which were previously considered undesirable, and modern data processing algorithms have opened up new prospects for metal oxide gas sensors in non-critical applications. It is safe to assume that the use of such approaches will continue to develop and will bring the creation of full-fledged “electronic nose” systems and “smart sensors” closer than ever before.

6. Conclusions

This article highlights recent advances in the field of semiconductor metal oxide gas sensors for environmental monitoring (especially H_2 , CO_x , NO_x , SO_x , and CH_4 gases), underlines important factors that complicate the development of gas sensors, and discusses the development of old and new solutions to these problems. The paper demonstrates the extent of recent advances in the most common SMO sensors due to their high sensitivity, ease of fabrication, ultra-small size, and cost effectiveness. In particular, it is emphasized that 1D MOx nanostructures have significant potential for use in the next generation of chemical sensors that will be very small, low power, inexpensive, and more sensitive than existing commercial sensors. It is noted that recent research has aimed to develop low-temperature sensors based on materials with high surface area and composites of metal oxides with other metal oxides, carbon or polymeric materials, MOFs, etc.

For instance, according to the literature review, semiconducting metal oxides like SnO_2 , ZnO , TiO_2 , and NiO are frequently studied as sensing layers for chemoresistive gas sensors to monitor gases such as H_2 , CO_x , SO_x , NO_x , and CH_4 in the environment. Herewith, the increase in sensitivity and the reduction in the operating temperature can be achieved via metal oxide decoration or creating metal oxide-based nanomaterials/nanocomposites. Hydrothermal synthesis is the most frequently used approach to produce metal oxides. Research on room-temperature sensors based on metal oxides is increasing. The sensors can achieve a response of 100 or more with short response and recovery times of up to 10 to 20 s, respectively. This shows that researchers are making significant progress in developing highly sensitive, selective, miniaturized, and energy-efficient sensors based on metal oxides. However, there are still some challenges in the development of metal oxide gas sensors. For instance, the selectivity issue is often overlooked by researchers and not often considered in scientific articles, remaining one of the main drawbacks of metal oxide sensors. Furthermore, insufficient lifetimes and challenges in creating optimal geometric characteristics require further in-depth studies to develop sensor devices with the desired design and at reduced fabrication times. In addition to the material's properties, the electrode spacing, electrode width, and electrode position can also significantly contribute to the response of gas sensors. Accordingly, the configurations and geometry of SMO sensors have been analyzed in the manuscript. It has been concluded that among different electrode configurations, including cylindrical, disk-type, interdigitated, and memristor-type, interdigitated and memristor-type are the most widely accepted due to the possibility of enhancing sensor performance by altering the electrode's geometry.

The sensitivity mechanisms of sensors and the factors that affect their performance are broad topics that are difficult to cover concisely. Therefore, only the main aspects of the gas-sensing process in metal oxide sensors have been identified and briefly described, such as the oxygen adsorption and chemisorption model, and the influence of operating temperature, humidity, and surface morphology. Despite being researched for a long time, there is still much effort being made to ensure metal oxide sensors work efficiently at room temperature and obtain the most optimal surface structure for sensitive oxides. Some of the studies reviewed in this paper have shown excellent results, demonstrating that significant progress is being made in this direction. Sophisticated nanostructures and sensors that effectively sense a wide range of gases at low temperatures have been developed.

The clever utilization of nonlinearity and cross-selectivity effects, previously considered undesirable, along with modern data processing algorithms have brought new opportunities for metal oxide gas sensors. It is reasonable to assume that the use of these approaches will continue to evolve and will bring us closer than ever to creating fully fledged “electronic nose” systems and “smart sensors”. Considering the complex composition of most air pollutants, multisensory systems are promising devices for environmental monitoring, including air quality assessment, gas detection, the quantification of specific compounds, and control processes. The employment of such systems allows us to overcome the insufficient selectivity of single-semiconductor metal oxide sensors; however, specifically developed and fine-tuned data-processing tools are required to obtain reliable results with high accuracy for real-time continuous environmental monitoring.

Author Contributions: M.T.: writing—original draft preparation; T.D.: writing—original draft preparation; visualization; writing—review and editing; supervision; B.S.: supervision, project administration, validation, visualization, writing—review and editing; S.K.: writing—original draft preparation; visualization; writing—review and editing. All authors have read and agreed to the published version of the manuscript.

Funding: This research received no external funding.

Data Availability Statement: Data sharing is not applicable to this article.

Conflicts of Interest: The authors declare no conflict of interest.

References

1. Uma, S.; Shobana, M.K. Metal oxide semiconductor gas sensors in clinical diagnosis and environmental monitoring. *Sens. Actuators A Phys.* **2023**, *349*, 114044. [[CrossRef](#)]
2. Dontsova, T.A.; Nahirniak, S.V.; Astrelin, I.M. Metaloxide nanomaterials and nanocomposites of ecological purpose. *J. Nanomater.* **2019**, *2019*, 5942194. [[CrossRef](#)]
3. Burgués, J.; Marco, S. Environmental chemical sensing using small drones: A review. *Sci. Total Environ.* **2020**, *748*, 141172. [[CrossRef](#)] [[PubMed](#)]
4. Zhang, C.; Zheng, Z. Electronic noses based on metal oxide semiconductor sensors for detecting crop diseases and insect pests. *Comput. Electron. Agric.* **2022**, *197*, 106988. [[CrossRef](#)]
5. Nahirniak, S.; Dontsova, T.; Lapinsky, A.; Tereshkov, M.; Singh, R. Soil and soil breathing remote monitoring: A short review. *Biosyst. Divers.* **2020**, *28*, 350–356. [[CrossRef](#)]
6. *Nanotechnology-Based E-Noses: Fundamentals and Emerging Applications*; Woodhead Publishing Series in Electronic and Optical Materials; Elsevier: Cambridge, UK, 2023; 457p.
7. An, Y.; Tian, Y.; Wei, C.; Tao, Y.; Xi, B.; Xiong, S.; Feng, J.; Qian, Y. Dealloying: An effective method for scalable fabrication of 0D, 1D, 2D, 3D materials and its application in energy storage. *Nano Today* **2021**, *37*, 101094. [[CrossRef](#)]
8. Galstyan, V.; Moumen, A.; Kumara, G.W.C.; Comini, E. Progress towards chemical gas sensors: Nanowires and 2D semiconductors. *Sens. Actuators B Chem.* **2022**, *357*, 131466. [[CrossRef](#)]
9. Ortiz-Casas, B.; Galdámez-Martínez, A.; Gutiérrez-Flores, J.; Ibañez, A.B.; Panda, P.K.; Santana, G.; de la Vega, H.A.; Suar, M.; Rodelo, C.G.; Kaushik, A.; et al. Bio-acceptable 0D and 1D ZnO nanostructures for cancer diagnostics and treatment. *Mater. Today* **2021**, *50*, 533–569. [[CrossRef](#)]
10. Nagirnyak, S.V.; Lutz, V.A.; Dontsova, T.; Astrelin, I.M. The effect of the synthesis conditions on morphology of tin (IV) oxide obtained by vapor transport method. In *Nanophysics, Nanophotonics, Surface Studies, and Applications*; Fesenko, O., Yatsenko, L., Eds.; Springer Proceedings in Physics; Springer: Berlin/Heidelberg, Germany, 2016; Volume 183, pp. 331–341.
11. Masuda, Y. Recent advances in SnO₂ nanostructure based gas sensors. *Sens. Actuators B Chem.* **2022**, *364*, 131876. [[CrossRef](#)]

12. Dey, A. Semiconductor metal oxide gas sensors: A review. *Mater. Sci. Eng. B* **2018**, *229*, 206–217. [[CrossRef](#)]
13. Kaur, N.; Singh, M.; Comini, E. One-dimensional nanostructured oxide chemoresistive sensors. *Langmuir* **2020**, *36*, 6326–6344. [[CrossRef](#)] [[PubMed](#)]
14. Nagirnyak, S.V.; Lutz, V.A.; Dontsova, T.A. Synthesis and characterization of tin (IV) oxide obtained by chemical vapor deposition method. *Nanoscale Res. Lett.* **2016**, *11*, 343. [[CrossRef](#)]
15. Chen, L.; Yu, Q.; Pan, C.; Song, Y.; Dong, H.; Xie, X.; Li, Y.; Liu, J.; Wang, D.; Chen, X. Chemiresistive gas sensors based on electrospun semiconductor metal oxides: A review. *Talanta* **2022**, *246*, 123527. [[CrossRef](#)]
16. Dontsova, T.A.; Nagirnyak, S.V.; Zhorov, V.V.; Yasiievych, Y.V. SnO₂ nanostructures: Effect of processing parameters on their structural and functional properties. *Nanoscale Res. Lett.* **2017**, *12*, 332. [[CrossRef](#)]
17. Paul, R.; Das, B.; Ghosh, R. Novel approaches towards design of metal oxide based hetero-structures for room temperature gas sensor and its sensing mechanism: A recent progress. *J. Alloys Compd.* **2023**, *941*, 168943. [[CrossRef](#)]
18. Wang, J.; Shen, H.; Xia, Y.; Komarneni, S. Light-activated room-temperature gas sensors based on metal oxide nanostructures: A review on recent advances. *Ceram. Int.* **2021**, *47*, 7353–7368. [[CrossRef](#)]
19. Latif, U.; Dickert, F.L. Graphene hybrid materials in gas sensing applications. *Sensors* **2015**, *15*, 30504–30524. [[CrossRef](#)]
20. Calise, F.; D'Accadia, M.D.; Santarelli, M.; Lanzini, A.; Ferrero, D. (Eds.) *Solar Hydrogen Production: Processes, Systems and Technologies*; Academic Press: Cambridge, MA, USA, 2019; 560p.
21. Nowotny, J.; Veziroglu, T.N. Impact of hydrogen on the environment. *Int. J. Hydrogen Energy* **2011**, *36*, 13218–13224. [[CrossRef](#)]
22. Xu, M.; Peng, B.; Zhu, X.; Guo, Y. Multi-gas detection system based on non-dispersive infrared (NDIR) spectral technology. *Sensors* **2022**, *22*, 836. [[CrossRef](#)] [[PubMed](#)]
23. Ravishankara, A.R.; Daniel, J.S.; Portmann, R.W. Nitrous oxide (N₂O): The dominant ozone-depleting substance emitted in the 21st century. *Science* **2009**, *326*, 123–125. [[CrossRef](#)] [[PubMed](#)]
24. OECD. *Environment at a Glance 2013: OECD Indicators*; OECD Publishing: Paris, France, 2013; 108p. [[CrossRef](#)]
25. Dhall, S.; Mehta, B.R.; Tyagi, A.K.; Sood, K. A review on environmental gas sensors: Materials and technologies. *Sens. Int.* **2021**, *2*, 100116. [[CrossRef](#)]
26. Kholod, N.; Evans, M.; Pilcher, R.C.; Roshchanka, V.; Ruiz, F.; Côté, M.; Collings, R. Global methane emissions from coal mining to continue growing even with declining coal production. *J. Clean. Prod.* **2020**, *256*, 120489. [[CrossRef](#)]
27. Sachin, N.; Sanjit, M.; Ali, M.; Sang, K. Metal oxide ceramic gas sensors. *Encycl. Mater. Electron.* **2023**, *1*, 452–462.
28. Nikolić, M.; Milovanović, V.; Vasiljevic, Z.; Stamenkovic, Z. Semiconductor gas sensors: Materials, technology, design and application. *Sensors* **2020**, *2020*, 6694. [[CrossRef](#)]
29. Zhu, L.-Y.; Ou, L.-X.; Mao, L.-W.; Wu, X.; Liu, Y.; Lu, H.-L. Advances in noble metal-decorated metal oxide nanomaterials for chemiresistive gas sensors: Overview. *Nano-Micro Lett.* **2023**, *15*, 89. [[CrossRef](#)]
30. Sohal, M.K.; Mahajan, A.; Gasso, S.; Nahirniak, S.V.; Dontsova, T.A.; Singh, R.C. Rare earth-tuned oxygen vacancies in gadolinium-doped tin oxide for selective detection of volatile organic compounds. *J. Mater. Sci. Mater. Electron.* **2020**, *31*, 8446–8455. [[CrossRef](#)]
31. Zegebreal, L.T.; Tegegne, N.A.; Hone, F.G. Recent progress in hybrid conducting polymers and metal oxide nanocomposite for room-temperature gas sensor applications: A Review. *Sens. Actuators A Phys.* **2023**, *359*, 114472. [[CrossRef](#)]
32. Bhati, V.S.; Kumar, M.; Banerjee, R. Gas sensing performance of 2D nanomaterials/metal oxide nanocomposites: A review. *J. Mater. Chem. C* **2021**, *9*, 8776–8806. [[CrossRef](#)]
33. Potyrailo, R.A.; Go, S.; Sexton, D.; Li, X.; Alkadi, N.; Kolmakov, A.; Amm, B.; St-Pierre, R.; Scherer, B.; Nayeri, M.; et al. Extraordinary performance of semiconducting metal oxide gas sensors using dielectric excitation. *Nat. Electron.* **2020**, *3*, 280–289. [[CrossRef](#)]
34. Gu, H.; Wang, Z.; Hu, Y. Hydrogen gas sensors based on semiconductor oxide nanostructures. *Sensors* **2012**, *12*, 5517–5550. [[CrossRef](#)] [[PubMed](#)]
35. Ren, Q.; Cao, Y.-Q.; Arulraj, D.; Liu, C.; Wu, D.; Li, W.; Li, A. Review—Resistive-type hydrogen sensors based on zinc oxide nanostructures. *J. Electrochem. Soc.* **2020**, *167*, 067528. [[CrossRef](#)]
36. Hossain, M.K.; Drmosh, Q.A. Noble metal-decorated nanostructured zinc oxide: Strategies to advance chemiresistive hydrogen gas sensing. *Chem. Rec.* **2022**, *22*, e202200090. [[CrossRef](#)] [[PubMed](#)]
37. Dontsova, T.; Yanushevskaya, O.; Nahirniak, S.; Kutuzova, A.; Krynets, G.; Smertenko, P. Characterization of commercial TiO₂ P90 modified with ZnO by the impregnation method. *J. Chem.* **2021**, *2021*, 9378490. [[CrossRef](#)]
38. Nahirniak, S.V.; Dontsova, T.A.; Chen, Q. Sensing properties of SnO₂-MWCNTs nanocomposites towards H₂. *Mol. Cryst. Liq. Cryst.* **2018**, *674*, 48–58. [[CrossRef](#)]
39. Chang, C.W.; Liu, I.P.; Yao, P.C.; Lin, K.W.; Hsu, W.C.; Liu, W.C. Hydrogen detecting characteristics of a palladium nanoparticle/indium gallium oxide based sensor. *Sens. Actuators B Chem.* **2023**, *393*, 134240. [[CrossRef](#)]
40. Nguyen, T.T.D.; Dao, D.V.; Kim, D.S.; Lee, H.L.; Oh, S.Y.; Lee, I.H.; Yu, Y.T. Effect of core and surface area toward hydrogen gas sensing performance using Pd@ZnO core-shell nanoparticles. *J. Colloid Interface Sci.* **2021**, *587*, 252–259. [[CrossRef](#)] [[PubMed](#)]
41. Le, H.J.; Dao, V.D.; Yu, Y.T. Superfast and efficient hydrogen gas sensor using PdAu alloy@ZnO core-shell nanoparticles. *J. Mater. Chem. A* **2020**, *8*, 12968–12974. [[CrossRef](#)]
42. Hübert, T.; Boon-Brett, L.; Black, V.; Banach, U. Hydrogen sensors—A review. *Sens. Actuators B Chem.* **2011**, *157*, 329–352. [[CrossRef](#)]

43. Kim, S.H.; Yun, K.S. Room-temperature hydrogen gas sensor composed of palladium thin film deposited on NiCo₂O₄ nanoneedle forest. *Sens. Actuators B Chem.* **2023**, *376*, 132958. [[CrossRef](#)]
44. Luo, Y.; Zhang, C.; Zheng, B.; Geng, X.; Debliquy, M. Hydrogen sensors based on noble metal doped metal-oxide semiconductor: A review. *Int. J. Hydrogen Energy* **2017**, *42*, 20386–20397. [[CrossRef](#)]
45. Zhang, C.; Xu, K.; Liu, K.; Xu, J.; Zheng, Z. Metal oxide resistive sensors for carbon dioxide detection. *Coord. Chem. Rev.* **2022**, *472*, 214758. [[CrossRef](#)]
46. Lupan, O.; Chow, L.; Shishiyanu, S.; Monaico, E.; Shishiyanu, T.; Sontea, V.; Cuenya, B.R.; Naitabdi, A.; Park, S.; Schulte, A. Nanostructured zinc oxide films synthesized by successive chemical solution deposition for gas sensor applications. *Mater. Res. Bull.* **2009**, *44*, 63–69. [[CrossRef](#)]
47. Kanaparthi, S.; Singh, V. Chemiresistive sensor based on zinc oxide nanoflakes for CO₂ detection. *ACS Appl. Nano Mater.* **2019**, *2*, 700–706. [[CrossRef](#)]
48. Mahajan, S.; Jagtap, S. Metal-oxide semiconductors for carbon monoxide (CO) gas sensing: A review. *Appl. Mater. Today* **2020**, *18*, 100483. [[CrossRef](#)]
49. Fine, G.F.; Cavanagh, L.M.; Afonja, A.; Binions, R. Metal oxide semi-conductor gas sensors in environmental monitoring. *Sensors* **2010**, *10*, 5469–5502. [[CrossRef](#)] [[PubMed](#)]
50. Tereshkov, M.; Dontsova, T.; Yanushevskaya, O.; Dusheiko, M.; Smertenko, P. Solution composition and temperature impact on physicochemical properties of synthesized zinc oxide. *Appl. Nanosci.* **2022**, *12*, 2523–2532. [[CrossRef](#)]
51. Bagheri, F.; Haratizadeh, H. UV-activated CO₂ sensor based on ZnO nanoparticles at low temperatures. *Mater. Sci. Semicond. Process.* **2022**, *141*, 106422. [[CrossRef](#)]
52. Zhou, Q.; Zeng, W.; Chen, W.; Xu, L.; Kumar, R.; Umar, A. High sensitive and low-concentration sulfur dioxide (SO₂) gas sensor application of heterostructure NiO-ZnO nanodisks. *Sens. Actuators B Chem.* **2019**, *298*, 126870. [[CrossRef](#)]
53. Tyagi, P.; Sharma, A.; Tomar, M.; Gupta, V. Metal oxide catalyst assisted SnO₂ thin film based SO₂ gas sensor. *Sens. Actuators B Chem.* **2016**, *224*, 282–289. [[CrossRef](#)]
54. Pan, Q.; Yang, Z.; Wang, W.; Zhang, D. Sulfur dioxide gas sensing at room temperature based on tin selenium/tin dioxide hybrid prepared via hydrothermal and surface oxidation treatment. *Rare Met.* **2020**, *40*, 1588–1596. [[CrossRef](#)]
55. Chaitra, U.; Ali, A.; Viegas, A.E.; Kekuda, D.; Rao, K.M. Growth and characterization of undoped and aluminium doped zinc oxide thin films for SO₂ gas sensing below threshold value limit. *Appl. Surf. Sci.* **2019**, *496*, 143724. [[CrossRef](#)]
56. Tyagi, P.; Sharma, A.; Tomar, M.; Gupta, V. Efficient detection of SO₂ gas using SnO₂ based sensor loaded with metal oxide catalysts. *Procedia Eng.* **2014**, *87*, 1075–1078. [[CrossRef](#)]
57. Kang, X.; Deng, N.; Yan, Z.; Pan, Y.; Sun, W.; Zhang, Y. Resistive-type VOCs and pollution gases sensor based on SnO₂: A review. *Mater. Sci. Semicond. Process.* **2022**, *138*, 106246. [[CrossRef](#)]
58. Fu, Y.; Li, J.; Xu, H. SnO₂ recycled from tin slime for enhanced SO₂ sensing properties by NiO surface decoration. *Mater. Sci. Semicond. Process.* **2020**, *114*, 105073. [[CrossRef](#)]
59. Stoycheva, T.; Vallejos, S.; Blackman, C.S.; Moniz, S.J.A.; Calderer, J.; Correig, X. Important considerations for effective gas sensors based on metal oxide nanoneedles films. *Sens. Actuators B Chem.* **2012**, *161*, 406–413. [[CrossRef](#)]
60. Liu, H.; Wan, J.; Fu, Q.; Li, M.; Luo, W.; Zheng, Z.; Cao, H.; Hu, Y.; Zhou, D. Tin oxide films for nitrogen dioxide gas detection at low temperatures. *Sens. Actuators B Chem.* **2013**, *177*, 460–466. [[CrossRef](#)]
61. Liu, T.; Jia, X.; Qiao, L.; Yang, J.; Wang, S.; Li, Y.; Shao, D.; Feng, L.; Song, H. Conductometric NO₂ gas sensors achieved by design of Ti₃C₂T_x@ZnO heterostructures for application around 80 °C. *Sens. Actuators B Chem.* **2023**, *390*, 133908. [[CrossRef](#)]
62. Afzal, A.; Cioffi, N.; Sabbatini, L.; Torsi, L. NO_x sensors based on semiconducting metal oxide nanostructures: Progress and perspectives. *Sens. Actuators B Chem.* **2012**, *171–172*, 25–42. [[CrossRef](#)]
63. Sohal, M.K.; Mahajan, A.; Gasso, S.; Nahirniak, S.; Dontsova, T. Modification of SnO₂ surface oxygen vacancies through Er doping for ultralow NO₂ detection. *Mater. Res. Bull.* **2020**, *133*, 111051. [[CrossRef](#)]
64. Srivastava, S. Study of gas sensor detection for NO_x Gas: A review. *Mater. Today Proc.* **2021**, *37*, 3709–3712. [[CrossRef](#)]
65. Trung, T.D.; Toan, N.V.; Tong, P.V.; Duy, N.V.; Hoa, N.D.; Hieu, N.V. Synthesis of single-crystal SnO₂ nanowires for NO_x gas sensors application. *Ceram. Int.* **2012**, *38*, 6557–6563. [[CrossRef](#)]
66. Zhao, S.; Shen, Y.; Zhou, P.; Hao, F.; Xu, X.; Gao, S.; Wei, D.; Ao, Y.; Shen, Y. Enhanced NO₂ sensing performance of ZnO nanowires functionalized with ultra-fine In₂O₃ nanoparticles. *Sens. Actuators B Chem.* **2020**, *308*, 127729. [[CrossRef](#)]
67. Kang, Y.; Yu, F.; Zhang, L.; Wang, W.; Chen, L.; Li, Y. Review of ZnO-based nanomaterials in gas sensors. *Solid State Ion.* **2021**, *360*, 115544. [[CrossRef](#)]
68. Lux, K.C.; Hot, J.; Fau, P.; Bertron, A.; Kahn, M.L.; Ringot, E.; Fajerweg, K. Nano-gold decorated ZnO: An alternative photocatalyst promising for NO_x degradation. *Chem. Eng. Sci.* **2023**, *267*, 118377.
69. Nundy, S.; Eom, T.; Kang, J.; Suh, J.; Cho, M.; Park, J.S.; Lee, H.J. Flower-shaped ZnO nanomaterials for low-temperature operations in NO_x gas sensors. *Ceram. Int.* **2020**, *46*, 5706–5714. [[CrossRef](#)]
70. Xia, Y.; Xu, L.; He, S.; Zhou, L.; Wang, M.; Wang, J.; Komarneni, S. UV-activated WS₂/SnO₂ 2D/0D heterostructures for fast and reversible NO₂ gas sensing at room temperature. *Sens. Actuators B Chem.* **2022**, *364*, 131903. [[CrossRef](#)]
71. Chakrabarty, P.; Banik, M.; Gogurla, N.; Santra, S.; Ray, S.K.; Mukherjee, R. Light trapping-mediated room-temperature gas sensing by ordered ZnO nano structures decorated with plasmonic Au nanoparticles. *ACS Omega* **2019**, *4*, 12071–12080. [[CrossRef](#)]

72. Chen, R.; Wang, J.; Xia, Y.; Xiang, L. Near infrared light enhanced room-temperature NO₂ gas sensing by hierarchical ZnO nanorods functionalized with PbS quantum dots. *Sens. Actuators B Chem.* **2018**, *255*, 2538–2545. [[CrossRef](#)]
73. Peterson, P.J.D.; Aujla, A.; Grant, K.H.; Brundle, A.G.; Thompson, M.R.; Hey, J.V.; Leigh, R.J. Practical use of metal oxide semiconductor gas sensors for measuring nitrogen dioxide and ozone in urban environments. *Sensors* **2017**, *17*, 1653. [[CrossRef](#)]
74. Aldhafeeri, T.R.; Fowler, M.; Vrolyk, R.; Pope, M.A.; Fowler, M. A review of methane gas detection sensors: Recent developments and future perspectives. *Inventions* **2020**, *5*, 28. [[CrossRef](#)]
75. Basu, S.; Basu, P.K. Nanocrystalline metal oxides for methane sensors: Role of noble metals. *J. Sens.* **2009**, *2009*, 861968. [[CrossRef](#)]
76. De Lacy Costello, B.P.J.; Ewen, R.J.; Ratcliffe, N.M.; Richards, M. Highly sensitive room temperature sensors based on the UV-LED activation of zinc oxide nanoparticles. *Sens. Actuators B Chem.* **2008**, *134*, 945–952. [[CrossRef](#)]
77. Aghagoli, Z.; Ardyanian, M. Synthesis and study of the structure, magnetic, optical and methane gas sensing properties of cobalt doped zinc oxide microstructures. *J. Mater. Sci. Mater. Electron.* **2018**, *29*, 7130–7141. [[CrossRef](#)]
78. Bhattacharyya, P.; Basu, P.K.; Saha, H.; Basu, S. Fast response methane sensor using nanocrystalline zinc oxide thin films derived by sol–gel method. *Sens. Actuators B Chem.* **2007**, *124*, 62–67. [[CrossRef](#)]
79. Wang, Y.; Meng, X.; Yao, M.; Sun, G.; Zhang, Z. Enhanced CH₄ sensing properties of Pd modified ZnO nanosheets. *Ceram. Int.* **2019**, *45*, 13150–13157. [[CrossRef](#)]
80. Li, H.Y.; Shu-Na, Z.; Zang, S.Q.; Li, J. Functional metal–organic frameworks as effective sensors of gases and volatile compounds. *Chem. Soc. Rev.* **2020**, *49*, 6364–6401. [[CrossRef](#)]
81. Yuan, Z.; Han, E.; Meng, F.; Zuo, K. Detection and identification of volatile organic compounds based on temperature-modulated ZnO sensors. *IEEE Trans. Instrum. Meas.* **2020**, *69*, 4533–4544. [[CrossRef](#)]
82. Luan, Z.; Zeng, W.; Li, Y. A non-oxygen adsorption mechanism for hydrogen detection of nanostructured SnO₂ based sensors. *Mater. Res. Bull.* **2019**, *109*, 108–116.
83. Choi, K.-S.; Chang, S.-P. Effect of structure morphologies on hydrogen gas sensing by ZnO nanotubes. *Mater. Lett.* **2018**, *230*, 48–52. [[CrossRef](#)]
84. Kumar, M.; Kumar, R.; Rajamani, S.; Ranwa, S.; Fanetti, M.; Valant, M.; Kumar, M. Efficient room temperature hydrogen sensor based on UV-activated ZnO nano-network. *Nanotechnology* **2017**, *28*, 365502. [[CrossRef](#)]
85. Fan, F.; Zhang, J.; Li, J.; Zhang, N.; Hong, R.; Deng, X.; Tang, P.; Li, D. Hydrogen sensing properties of Pt-Au bimetallic nanoparticles loaded on ZnO nanorods. *Sens. Actuators B Chem.* **2017**, *241*, 895–903. [[CrossRef](#)]
86. Geng, X.; Luo, Y.; Zheng, B.; Zhang, C. Photon assisted room-temperature hydrogen sensors using PdO loaded WO₃ nanohybrids. *Int. J. Hydrogen Energy* **2017**, *42*, 6425–6434. [[CrossRef](#)]
87. Mobtakeran, S.; Habashyani, S.; Çoban, Ö.; Budak, H.F.; Kasapoğlu, A.E.; Gür, E. Effect of growth pressure on sulfur content of RF-magnetron sputtered WS₂ films and thermal oxidation properties of them toward using Pd decorated WO₃ based H₂ gas sensor. *Sens. Actuators B Chem.* **2023**, *381*, 133485. [[CrossRef](#)]
88. Li, G.; Du, K.; Wang, X.; Wang, X.; Chen, B.; Qiu, C.; Xu, J. Pd nanoparticles decorated SnO₂ ultrathin nanosheets for highly sensitive H₂ sensor: Experimental and theoretical studies. *Int. J. Hydrogen Energy* **2023**, *50*, 761–771. [[CrossRef](#)]
89. Song, Z.; Zhang, L.; Zhou, Q.; Zhang, Z.; Dong, Z.; Nie, L.; Liu, Q.; Pan, G. In-Situ synthesis of needle-like PdO-decorated NiO thin films on Al₂O₃ substrates for high-performance H₂ sensors. *Ceram. Int.* **2022**, *48*, 31746–31754. [[CrossRef](#)]
90. Karuppasamy, K.; Sharma, A.; Vikraman, D.; Lee, Y.A.; Sivakumar, P.; Korvink, J.G.; Kim, H.S.; Sharma, B. Room-temperature response of MOF-derived Pd@PdO core shell/γ-Fe₂O₃ microcubes decorated graphitic carbon based ultrasensitive and highly selective H₂ gas sensor. *J. Colloid Interface Sci.* **2023**, *652*, 692–704. [[CrossRef](#)] [[PubMed](#)]
91. More, M.S.; Bodkhe, G.A.; Ingle, N.N.; Singh, F.; Tsai, M.L.; Kim, M.; Shirsat, M.D. Metal-organic framework (MOF)/reduced graphene oxide (rGO) composite for high performance CO sensor. *Solid-State Electron.* **2023**, *204*, 108638. [[CrossRef](#)]
92. Krivetskiy, V.; Efitorov, A.; Arkhipenko, A.; Vladimirova, S.; Rumyantseva, M.; Dolenko, S.; Gaskov, A. Selective detection of individual gases and CO/H₂ mixture at low concentrations in air by single semiconductor metal oxide sensors working in dynamic temperature mode. *Sens. Actuators B Chem.* **2018**, *254*, 502–513. [[CrossRef](#)]
93. Fort, A.; Mugnaini, M.; Rocchi, S.; Vignoli, V.; Comini, E.; Faglia, G.; Ponzoni, A. Metal-oxide nanowire sensors for CO detection: Characterization and modeling. *Sens. Actuators B Chem.* **2010**, *148*, 283–291. [[CrossRef](#)]
94. Brosha, E.L.; Mukundan, R.; Brown, D.R.; Garzon, F.H.; Visser, J.H.; Zanini, M.; Zhou, Z.; Logothetis, E.M. CO/HC sensors based on thin films of LaCoO₃ and La_{0.8}Sr_{0.2}CoO_{3-δ} metal oxides. *Sens. Actuators B Chem.* **2000**, *69*, 171–182. [[CrossRef](#)]
95. Wang, D.; Zhang, D.; Pan, Q.; Wang, T.; Chen, F. Gas sensing performance of carbon monoxide sensor based on rod-shaped tin diselenide/MOFs derived zinc oxide polyhedron at room temperature. *Sens. Actuators B Chem.* **2022**, *371*, 132481. [[CrossRef](#)]
96. Wu, R.; Tian, L.; Li, H.; Liu, H.; Luo, J.; Tian, X.; Hua, Z.; Wu, Y.; Fan, S. A selective methane gas sensor based on metal oxide semiconductor equipped with an on-chip microfilter. *Sens. Actuators B Chem.* **2022**, *359*, 131557. [[CrossRef](#)]
97. Shwetha, H.R.; Sharath, S.M.; Guruprasad, B.; Rudraswamy, S.B. MEMS based metal oxide semiconductor carbon dioxide gas sensor. *Micro Nano Eng.* **2022**, *16*, 100156. [[CrossRef](#)]
98. Keerthana, S.; Rathnakannan, K. Room temperature operated carbon dioxide sensor based on silver doped zinc oxide/cupric oxide nanoflowers. *Sens. Actuators B Chem.* **2023**, *378*, 133181. [[CrossRef](#)]
99. Thomas, T.; Kumar, Y.; Ramón, J.A.R.; Agarwal, V.; Guzmán, S.S.; Pushpan, R.R.S.; Loredó, S.L.; Sanal, K.C. Porous silicon/α-MoO₃ nanohybrid based fast and highly sensitive CO₂ gas sensors. *Vacuum* **2021**, *184*, 109983. [[CrossRef](#)]

100. Miao, F.; Wu, H.; Tao, B.; Zang, Y. A passive-chipless LC carbon dioxide sensor with non-contact ZnO/CuO/RGO nanocomposites at room temperature. *Vacuum* **2023**, *215*, 112261. [[CrossRef](#)]
101. Wang, X.; Su, J.; Chen, H.; Li, G.; Shi, Z.; Zou, H.; Zou, X. Ultrathin In₂O₃ nanosheets with uniform mesopores for highly sensitive nitric oxide detection. *ACS Appl. Mater. Interfaces* **2017**, *9*, 16335–16342. [[CrossRef](#)]
102. Liu, B.; Luo, Y.; Li, K.; Wang, H.; Gao, L.; Duan, G. Room-temperature NO₂ gas sensing with ultra-sensitivity activated by ultraviolet light based on SnO₂ monolayer array film. *Adv. Mater. Interfaces* **2019**, *6*, 1900376. [[CrossRef](#)]
103. Shen, Y.; Zhong, X.; Zhang, J.; Li, T.; Zhao, S.; Cui, B.; Wei, D.; Zhang, Y.; Wei, K. In-situ growth of mesoporous In₂O₃ nanorod arrays on a porous ceramic substrate for ppb-level NO₂ detection at room temperature. *Appl. Surf. Sci.* **2019**, *498*, 143873. [[CrossRef](#)]
104. Hu, J.; Zou, C.; Su, Y.; Li, M.; Ye, X.; Cai, B.; Kong, E.S.-W.; Liu, Y. Light-assisted recovery for a highly-sensitive NO₂ sensor based on RGO-CeO₂ hybrids. *Sens. Actuators B Chem.* **2018**, *270*, 119–129. [[CrossRef](#)]
105. Chinh, N.D.; Quang, N.D.; Lee, H.; Hien, T.T.; Hieu, N.M.; Kim, D.; Kim, C.; Kim, D. NO gas sensing kinetics at room temperature under UV light irradiation of In₂O₃ nanostructures. *Sci. Rep.* **2016**, *6*, 3506. [[CrossRef](#)]
106. Zhang, Q.; Xie, G.; Xu, M.; Su, Y.; Tai, H.; Du, H.; Jiang, Y. Visible light-assisted room temperature gas sensing with ZnO-Ag heterostructure nanoparticles. *Sens. Actuators B Chem.* **2018**, *259*, 269–281. [[CrossRef](#)]
107. Wang, C.Y.; Hong, Z.S.; Wu, R.J. Promotion effect of Pt on a SnO₂-WO₃ material for NO_x sensing. *Phys. E Low-Dimens. Syst. Nanostructures* **2015**, *69*, 191–197. [[CrossRef](#)]
108. Cao, Z.; Gao, Q.; Zhou, M.; Li, X.; Wang, Q. LaNiTiO₃-SE-based stabilized zirconium oxide mixed potentiometric SO₂ gas sensor. *Ceram. Int.* **2022**, *48*, 9269–9276. [[CrossRef](#)]
109. Zeng, S.; Zhang, Y.; Zhang, Y.; Li, Y.; Tang, C.; Li, K.; Sun, J.; Deng, T. A novel room temperature SO₂ gas sensor based on TiO₂/rGO buried-gate FET. *Microelectron. Eng.* **2022**, *263*, 111841. [[CrossRef](#)]
110. Zhang, B.; Sun, J.; Gao, P.-X. Single bimodular sensor for differentiated detection of multiple oxidative gases. *Adv. Mater. Technol.* **2020**, *5*, 1901152. [[CrossRef](#)]
111. Manikandan, V.; Vigneselvan, S.; Petrila, L.; Mane, R.S.; Singh, A.; Sobczak, K.; Chandrasekaran, J. Long-lasting stability and low-concentration SO₂ gas detection aptitude of Sn-doped alumina sensors. *Mater. Chem. Phys.* **2022**, *291*, 126691.
112. Li, R.; Wang, S.; Li, S.; Zhao, F.; Dong, T.; He, P.; Yu, L.; Miao, J.; Fan, X. Cu-doped flower-like SnO₂ architecture toward promoting SO₂ detection: Fast equilibrium and low trace monitoring. *Sens. Actuators B Chem.* **2023**, *390*, 133953. [[CrossRef](#)]
113. Boudiba, A.; Zhang, C.; Bittencourt, C.; Umek, P.; Olivier, M.G.; Snyders, R.; Debliquy, M. SO₂ Gas Sensors based on WO₃ nanostructures with different morphologies. *Procedia Eng.* **2012**, *47*, 1033–1036. [[CrossRef](#)]
114. Nguyen, T.V.; Luong, N.A.; Nguyen, V.T.; Pham, A.T.; Le, A.T.; To, T.L.; Nguyen, V.Q. Effect of the phase composition of iron oxide nanorods on SO₂ gas sensing performance. *Mater. Res. Bull.* **2021**, *134*, 111087. [[CrossRef](#)]
115. Das, S.; Girija, K.G.; Debnath, A.K.; Vatsa, R.K. Enhanced NO₂ and SO₂ sensor response under ambient conditions by polyol synthesized Ni doped SnO₂ nanoparticles. *J. Alloys Compd.* **2021**, *854*, 157276. [[CrossRef](#)]
116. Thangamani, G.J.; Pasha, S.K.K. Titanium dioxide (TiO₂) nanoparticles reinforced polyvinyl formal (PVF) nanocomposites as chemiresistive gas sensor for sulfur dioxide (SO₂) monitoring. *Chemosphere* **2021**, *275*, 129960. [[CrossRef](#)] [[PubMed](#)]
117. He, X.; Ying, Z.; Wen, F.; Li, L.; Zheng, X.; Zheng, P.; Wang, G. MoS₂-doped spherical SnO₂ for SO₂ sensing under UV light at room temperature. *Mater. Sci. Semicond. Process.* **2021**, *134*, 105997. [[CrossRef](#)]
118. Wang, Y.; Cui, Y.; Meng, X.; Zhang, Z.; Cao, J. A gas sensor based on Ag-modified ZnO flower-like microspheres: Temperature-modulated dual selectivity to CO and CH₄. *Surf. Interfaces* **2021**, *24*, 101110. [[CrossRef](#)]
119. Zhang, H.; Wang, Y.; Sun, X.; Wang, Y.; Li, M.; Cao, J.; Qin, C. Enhanced CH₄ sensing performances of g-C₃N₄ modified ZnO nanospheres sensors under visible-light irradiation. *Mater. Res. Bull.* **2023**, *165*, 112290. [[CrossRef](#)]
120. Tshabalala, Z.P.; Swart, H.C.; Motaung, D.E. Fabrication of TiO₂ nanofibers based sensors for enhanced CH₄ performance induced by notable surface area and acid treatment. *Vacuum* **2021**, *187*, 110102. [[CrossRef](#)]
121. Han, L.; Zhang, S.; Zhang, B.; Zhang, B.; Wang, Y.; Bala, H.; Zhang, Z. Dual-selective detection of CO and CH₄ based on hierarchical porous In₂O₃ nanoflowers with Pd modification. *J. Mater.* **2022**, *8*, 545–555. [[CrossRef](#)]
122. Zhang, S.; Li, J.; Han, L.; Zhang, B.; Wang, Y.; Zhang, Z. Preparation of porous NiO/In₂O₃ nanoflower-like composites and their dual selectivity for CO/CH₄. *Mater. Res. Bull.* **2023**, *165*, 112332. [[CrossRef](#)]
123. Vatandoust, L.; Habibi, A.; Naghshara, H.; Sajedehe Mohammadi Aref, S.M. Fabrication and investigation of TiO_{1.5}/ZnO nanocomposite nanosensor for detection of CO and CH₄ gases. *Surf. Interfaces* **2022**, *31*, 102001. [[CrossRef](#)]
124. Mishra, V.N.; Agarwal, R.P. Sensitivity, response and recovery time of SnO₂ based thick-film sensor array for H₂, CO, CH₄ and LPG. *Microelectron. J.* **1998**, *29*, 861–874. [[CrossRef](#)]
125. Mounasamy, V.; Mani, G.K.; Ponnusamy, D.; Tsuchiya, K.; Reshma, P.R.; Prasad, A.K.; Madanagurusamy, S. Investigation on CH₄ sensing characteristics of hierarchical V₂O₅ nanoflowers operated at relatively low temperature using chemiresistive approach. *Anal. Chim. Acta* **2020**, *1106*, 148–160. [[CrossRef](#)]
126. Nahirniak, S.; Dontsova, T.; Astrelin, I. Directional synthesis of SnO₂-based nanostructures for use in gas sensors. In *Nanochemistry, Biotechnology, Nanomaterials, and Their Applications. NANO 2017*; Springer Proceedings in Physics; Springer: Berlin/Heidelberg, Germany, 2018; Volume 214, pp. 233–245.
127. Dontsova, T.; Nahirniak, S.; Linyucheva, O.; Tereshkov, M.; Mahajan, A.; Singh, R.C. Physicochemical properties of Tin (IV) oxide synthesized by different methods and from different precursors. *Appl. Nanosci.* **2022**, *12*, 1155–1168. [[CrossRef](#)]

128. Sviderskyi, A.; Nahirniak, S.; Yashchenko, T.; Dontsova, T.; Kalinowski, S. Properties of TiO₂ and SnO₂ in a state of different dispersion and morphology. In Proceedings of the NAP-2018, 2018 IEEE 8th International Conference on Nanomaterials: Applications and Properties (NAP), Zatoka, Ukraine, 9–14 September 2018; 01NNPT13-1-4.
129. Yashchenko, T.; Sviderskyi, A.; Nahirniak, S.; Dontsova, T.; Kalinowski, S. Electrical properties and sensitivity of SnO₂ nanostructures to organic compounds. *Nanosistemi Nanomater. Nanotehnologii* **2021**, *19*, 53–70.
130. Korotcenkov, G. Current trends in nanomaterials for metal oxide-based conductometric gas sensors: Advantages and limitations. Part 1: 1D and 2D Nanostructures. *Nanomaterials* **2020**, *10*, 1392. [[CrossRef](#)]
131. Xue, S.; Cao, S.; Huang, Z.; Yang, D.; Zhang, G. Improving gas-sensing performance based on MOS nanomaterials: A Review. *Materials* **2021**, *14*, 4263. [[CrossRef](#)] [[PubMed](#)]
132. Lee, D.; Chase, M.; Jung, J.; Kim, H.-D. Correlation between sensing accuracy and read margin of a memristor-based NO gas sensor array estimated by neural network analysis. *ACS Sens.* **2023**, *8*, 2105–2114. [[CrossRef](#)] [[PubMed](#)]
133. Kang, M.; Cho, I.; Park, J.; Jeong, J.; Lee, K.; Lee, B.; Henriquez, D.D.O.; Yoon, K.; Park, I. High accuracy real-time multi-gas identification by a batch-uniform gas sensor array and deep learning algorithm. *ACS Sens.* **2022**, *7*, 430–440. [[CrossRef](#)]
134. The Main Sources of Air Pollution. Available online: <https://www.breeze-technologies.de/blog/main-sources-of-air-pollution/> (accessed on 31 July 2023).
135. Capelli, L.; Sironi, S.; Del Rosso, R. Electronic noses for environmental monitoring applications. *Sensors* **2014**, *14*, 19979–20007. [[CrossRef](#)]
136. EN 13725:2003; Air Quality: Determination of Odor Concentration by Dynamic Olfactometry. Comitee Europeen de Normalisation: Brussels, Belgium, 2007.
137. Bourgeois, W.; Romain, A.-C.; Nicolas, J.; Stuetz, R.M. The use of sensor arrays for environmental monitoring: Interests and limitations. *J. Environ. Monit.* **2003**, *5*, 852–860. [[CrossRef](#)]
138. Betty, C.A.; Choudhury, S.; Girija, K.G. Reliability studies of highly sensitive and specific multi-gas sensor based on nanocrystalline SnO₂ film. *Sens. Actuators B* **2014**, *193*, 484–491. [[CrossRef](#)]
139. Abbas, M.N.; Moustafa, G.A.; Gopel, W. Multicomponent analysis of some environmentally important gases using semiconductor tin oxide sensors. *Anal. Chim. Acta* **2001**, *431*, 181–194. [[CrossRef](#)]
140. Özmet, A.; Dogan, E. Design of a portable e-nose instrument for gas classifications. *IEEE Trans. Instrum. Meas.* **2009**, *58*, 3609–3618.
141. Helli, O.; Siadat, M.; Lumbreras, M. Qualitative and quantitative identification of H₂S/NO₂ gaseous components in different reference atmospheres using a metal oxide sensor array. *Sens. Actuators B Chem.* **2004**, *103*, 403–408. [[CrossRef](#)]
142. Lee, D.S.; Jung, J.K.; Lim, J.W.; Huh, J.S.; Lee, D.D. Recognition of volatile organic compounds using SnO₂ sensor array and pattern recognition analysis. *Sens. Actuators B Chem.* **2001**, *77*, 228–236. [[CrossRef](#)]
143. Barisci, J.N.; Wallace, G.G.; Andrews, M.K.; Partridge, A.C.; Harris, P.D. Conduction polymer sensors for monitoring aromatic hydrocarbons using an electronic nose. *Sens. Actuators B Chem.* **2002**, *84*, 252–257. [[CrossRef](#)]
144. De Vito, S.; Massera, E.; Piga, A.; Martinotto, L.; di Francia, G. On field calibration of an electronic nose for benzene estimation in an urban pollution monitoring scenario. *Sens. Actuators B Chem.* **2008**, *129*, 750–757. [[CrossRef](#)]
145. Romain, A.-C.; Andre, P.; Nicolas, J. Three years experiment with the same tin oxide sensor array for identification of malodorous sources in the environment. *Sens. Actuators B* **2002**, *84*, 271–277. [[CrossRef](#)]
146. Cho, J.H.; Kim, Y.W.; Na, K.J.; Jeon, G.J. Wireless electronic nose system for real-time quantitative analysis of gas mixture using micro-gas sensor array and neuro-fuzzy network. *Sens. Actuators B Chem.* **2008**, *134*, 104–111. [[CrossRef](#)]
147. Dentoni, L.; Capelli, L.; Sironi, S.; del Rosso, R.; Zanetti, S.; Della Torre, M. Development of an electronic nose for environmental odour monitoring. *Sensors* **2012**, *12*, 14363–14381. [[CrossRef](#)]
148. Reddy, B.K.; Borse, P.H. Review—Recent material advances and their mechanistic approaches for room temperature chemiresistive gas sensors. *J. Electrochem. Soc.* **2021**, *168*, 057521. [[CrossRef](#)]
149. Dadkhan, M.; Tulliani, J.-M. Nanostructured metal oxide semiconductors towards greenhouse gas detection. *Chemosensors* **2022**, *10*, 57. [[CrossRef](#)]
150. Lee, S.P. Electrodes for semiconductor gas sensors. *Sensors* **2017**, *17*, 683. [[CrossRef](#)] [[PubMed](#)]
151. Adeyemo, A.; Mathew, J.; Jabir, A.; Di Natele, C.; Martinelli, E.; Ottavi, M. Efficient sensing approaches for high-density memristor sensor array. *J. Comput. Electron.* **2018**, *17*, 1285–1296. [[CrossRef](#)]
152. Liu, J.; Han, T.; Sun, B.; Kong, L.; Jin, Z.; Huang, X.; Liu, J.; Meng, F. Catalysis-based cataluminescent and conductometric gas sensors: Sensing nanomaterials, mechanism, applications and perspectives. *Catalysis* **2016**, *6*, 210.
153. Haidry, A.A.; Ebach-Stahl, A.; Saruhan, B. Effect of Pt/TiO₂ interface on room temperature hydrogen sensing performance of memristor type Pt/TiO₂/Pt structure. *Sens. Actuators B Chem.* **2017**, *253*, 1043–1054. [[CrossRef](#)]
154. Bhat, P.; Kumar, S.K.N. Evaluation of IDE-based flexible thin film ZnO sensor for VOC sensing in a custom designed gas chamber at room temperature. *J. Mater. Sci. Mater. Electron.* **2022**, *33*, 1529–1541. [[CrossRef](#)]
155. Mikolasek, M.; Meri, J.; Chymo, F.; Ondrejka, P.; Rehacek, V.; Predanocy, M.; Kostic, I.; Hotovy, I. Novel Cu₂O gas sensor prepared by potentiostatic electrodeposition on IDE electrodes. *J. Physics Conf. Ser.* **2019**, *1319*, 012009. [[CrossRef](#)]
156. Plecenik, T.; Moško, M.; Haidry, A.A.; Ďurina, P.; Truchlý, M.; Grančič, B.; Gregor, M.; Roch, T.; Satrapinskyy, L.; Mošková, A.; et al. Fast high-sensitive room-temperature semiconductor gas sensor based on nanoscale Pt-TiO₂-Pt sandwich. *Sens. Actuators B* **2015**, *207*, 351–361. [[CrossRef](#)]

157. Vidiš, M.; Plecenik, T.; Moškp, M.; Tomašec, S.; Roch, T.; Satrapinsky, L.; Grančič, B.; Plecenik, A. Gasistor: A memristor based gas-triggered switch and gas sensor with memory. *Appl. Phys. Lett.* **2019**, *115*, 093504. [[CrossRef](#)]
158. Nagirnyak, S.V.; Dontsova, T.A. Gas sensor device creation. In Proceedings of the NAP-2017, 2017 IEEE 7th International Conference on Nanomaterials: Applications and Properties (NAP), Odessa, Ukraine, 10–15 September 2017. 01NNPT13-1-4.
159. Feng, S.; Farha, F.; Li, Q.; Wan, Y.; Xu, Y.; Zhang, T.; Ning, H. Review on smart gas sensing technology. *Sensors* **2019**, *19*, 3760. [[CrossRef](#)]
160. Shaalan, N.M.; Yamazaki, T.; Kikuta, T. Effect of micro-electrode geometry on NO₂ gas-sensing characteristics of one-dimensional tin dioxide nanostructure microsensors. *Sens. Actuators B* **2011**, *156*, 784–790. [[CrossRef](#)]
161. Tamaki, J.; Mayaji, A.; Makinodan, J.; Ogura, S.; Konishi, S. Effect of micro-gap electrode on detection of dilute NO₂ using WO₃ thin film microsensors. *Sens. Actuators B Chem.* **2005**, *108*, 202–206. [[CrossRef](#)]
162. Nguyen Mihn, Q.; Tong, H.D.; Kuijk, A.; van de Bent, F.; Beekman, P.; van Rijn, C.J.M. Gas sensing performance at room temperature of nanogap interdigitated electrodes for detection of acetone at low concentration. *RSC Adv.* **2017**, *7*, 50279.
163. Miyaji, A.; Ogura, S.; Konishi, S.; Tamaki, J. Effect of micro-gap electrode in nitrogen dioxide sensor using tungsten oxide thin film. *Electrochem. Soc. Proc.* **2004**, *2004-09*, 201–204.
164. Prajesh, R.; Goyal, V.; Saini, V.; Bhargava, J.; Sharma, A.; Agarwal, A. Effect of IDE placement on response in metal oxide gas sensors. *Mater. Res. Express* **2018**, *5*, 096415. [[CrossRef](#)]
165. Ji, H.; Zeng, W.; Li, Y. Gas sensing mechanisms of metal oxide semiconductors: A focus review. *Nanoscale* **2019**, *11*, 22664–22684. [[CrossRef](#)]
166. Li, T.; Zeng, W.; Long, H.; Wang, Z. Nanosheet-assembled hierarchical SnO₂ nanostructures for efficient gas-sensing applications. *Sens. Actuators B Chem.* **2016**, *231*, 120–128. [[CrossRef](#)]
167. Xiao, X.; Liu, L.; Ma, J.; Ren, Y.; Cheng, X.; Zhu, Y.; Zhao, D.; Elzatahry, A.A.; Alghamdi, A.; Deng, Y. Ordered mesoporous tin oxide semiconductors with large pores and crystallized walls for high-performance gas sensing. *ACS Appl. Mater. Interfaces* **2018**, *10*, 1871–1880. [[CrossRef](#)]
168. Van Dang, T.; Hoa, N.D.; Van Duy, N.; Van Hieu, N. Chlorine gas sensing performance of on-chip grown ZnO, WO₃, and SnO₂ nanowire sensors. *ACS Appl. Mater. Interfaces* **2016**, *8*, 4828–4837. [[CrossRef](#)]
169. Yamazoe, N. New approaches for improving semiconductor gas sensors. *Sens. Actuators B Chem.* **1991**, *5*, 7–19. [[CrossRef](#)]
170. Ansari, S.G.; Boroojerdian, P.; Sainkar, S.R.; Karekar, R.N.; Aiyer, R.C.; Kulkarni, S.A. Grain size effects on H₂ gas sensitivity of thick film resistor using SnO₂ nanoparticles. *Thin Solid Film.* **1997**, *295*, 271–276. [[CrossRef](#)]
171. Baraton, M.-I.; Merhari, L. Influence of the particle size on the surface reactivity and gas sensing properties of SnO₂ nanopowders. *Mater. Trans.* **2001**, *42*, 1616–1622. [[CrossRef](#)]
172. Das, S.; Mojumder, S.; Saha, D.; Pal, M. Influence of major parameters on the sensing mechanism of semiconductor metal oxide based chemiresistive gas sensors: A review focused on personalized healthcare. *Sens. Actuators B Chem.* **2022**, *352*, 131066. [[CrossRef](#)]
173. Hwang, S.-H.; Kim, Y.K.; Hong, S.H.; Lim, S.K. Effect of the morphology and electrical property of metal-deposited ZNO nanostructures on CO gas sensitivity. *Nanomaterials* **2020**, *10*, 2124. [[CrossRef](#)] [[PubMed](#)]
174. Kim, K.; Choi, P.G.; Itoh, T.; Masuda, Y. Morphology control technique of ZnO by hydroxide ion supply rate and its effect on the ppt-level gas sensors. *J. Am. Ceram. Soc.* **2023**, *106*, 5944–5954. [[CrossRef](#)]
175. Yao, K.; Caruntu, D.I.; Cao, B.; O'Connor, C.J.; Zhou, W. Investigation of gas-sensing performance of SnO₂ nanoparticles with different morphologies. *IEEE Trans. Nanotechnol.* **2010**, *9*, 630–633. [[CrossRef](#)]
176. Xu, J.; Zhang, C. Oxygen vacancy engineering on cerium oxide nanowires for room-temperature linalool detection in rice aging. *J. Adv. Ceram.* **2022**, *11*, 1559–1570. [[CrossRef](#)]
177. Liu, J.; Chen, S.; Liu, Y.; Zhao, B. Progress in preparation, characterization, surface functional modification of graphene oxide: A review. *J. Saudi Chem. Soc.* **2022**, *26*, 101560. [[CrossRef](#)]
178. Bae, K.L.; Kim, J.; Lim, C.K.; Nam, K.M.; Song, H. Colloidal zinc oxide-copper(I) oxide nanocatalysts for selective aqueous photocatalytic carbon dioxide conversion into methane. *Nat. Commun.* **2017**, *8*, 1156. [[CrossRef](#)] [[PubMed](#)]
179. Lee, J.E.; Lim, C.K.; Park, H.J.; Song, H.; Choi, S.-Y.; Lee, D.-S. ZnO–CuO core-hollow cube nanostructures for highly sensitive acetone gas sensors at the ppb level. *ACS Appl. Mater. Interfaces* **2020**, *12*, 35688–35697. [[CrossRef](#)]
180. Yu, Q.; Kong, W.; Zhang, Y.; Li, X.; Xu, Y. Morphology-controllable synthesis of hierarchical hollow GaFeO₃ microcubes with selective triethylamine gas-sensing properties. *Ceram. Int.* **2022**, *48*, 4554–4562. [[CrossRef](#)]
181. Wang, C.-X.; Yin, L.; Zhang, L.; Xiang, D.; Gao, R. Metal oxide gas sensors: Sensitivity and influencing factors. *Sensors* **2010**, *10*, 2088–2106. [[CrossRef](#)]
182. Neri, G. First fifty years of chemoresistive gas sensors. *Chemosensors* **2015**, *3*, 1–20. [[CrossRef](#)]
183. Meixner, H.; Lampe, U. Metal oxide sensors. *Sens. Actuators B Chem.* **1996**, *33*, 198–202. [[CrossRef](#)]
184. Zhang, M.; Yuan, Z.; Shen, J.; Zheng, C. Improvement and mechanism for the fast response of a Pt/TiO₂ gas sensor. *Sens. Actuators B Chem.* **2010**, *148*, 87–92. [[CrossRef](#)]
185. Ghosh, A.; Maity, A.; Banerjee, R.; Majumder, S.B. Volatile organic compound sensing using copper oxide thin films: Addressing the cross sensitivity issue. *J. Alloys Compd.* **2017**, *692*, 108–118. [[CrossRef](#)]

186. Kamarudin, K.; Bennetts, V.H.; Mamduh, S.H.; Visvanathan, R.; Yeon, A.S.A.; Shakaff, A.Y.M.; Zakaria, A.; Abdullah, A.; Kamarudin, L.M. Cross-sensitivity of metal oxide gas sensor to ambient temperature and humidity: Effects on gas distribution mapping. *Am. Inst. Phys.* **2017**, *1808*, 020025.
187. Neri, G.; Leonardi, S.G.; Latino, M.; Donato, N.; Baek, S.; Conte, D.E.; Russo, P.A.; Pinna, N. Sensing behavior of SnO₂/reduced graphene oxide nanocomposites toward NO₂. *Sens. Actuators B Chem.* **2013**, *179*, 61–68. [[CrossRef](#)]
188. Fan, S.; Srivastava, A.K.; Dravid, V.P. UV-activated room-temperature gas sensing mechanism of polycrystalline ZnO. *Appl. Phys. Lett.* **2009**, *95*, 142106. [[CrossRef](#)]
189. Kumar, R.; Liu, X.; Zhang, J.; Kumar, M. Room-temperature gas sensors under photoactivation: From metal oxides to 2D materials. *Nano-Micro Lett.* **2020**, *12*, 164. [[CrossRef](#)]
190. Lee, J.H.; Kim, J.-Y.; Mirzaei, A.; Nam, M.-S.; Kim, H.W.; Kim, S.S. Room-temperature detection of acetone gas by PANI/NiO-loaded TiO₂ nanoparticles under UV irradiation. *Sens. Actuators B Chem.* **2023**, *374*, 132850. [[CrossRef](#)]
191. Pedowitz, M.; Kim, S.; Lewis, D.I.; Uppalapati, B.; Khan, D.; Bayram, F.; Koley, G.; Daniels, K.M. Fast selective sensing of nitrogen-based gases utilizing δ -MnO₂-epitaxial graphene-silicon carbide heterostructures for room temperature gas sensing. *J. Microelectromech. Syst.* **2020**, *29*, 846–852. [[CrossRef](#)]
192. Shin, D.H.; Choi, Y.S.; Park, S.-J.; Yeo, C.-S.; Park, Y.Y.; Jun, S.; Lee, S.-K.; Kim, T.-W.; Bae, S.; Hong, B.H. Fast and complete recovery of TMDs-decorated RGO fiber gas sensors at room temperature. *Appl. Surf. Sci.* **2022**, *578*, 151832. [[CrossRef](#)]
193. Moumen, A.; Kumarage, W.G.C.; Comini, E. P-type metal oxide semiconductor thin films: Synthesis and chemical sensor applications. *Sensors* **2022**, *22*, 1359. [[CrossRef](#)]
194. Abdullah, A.N.; Kamarudin, L.M.; Adom, A.H.; Zakaria, S.A.; Juffry, Z.H.M.; Bennetts, V.H. Correction model for metal oxide sensor drift caused by ambient temperature and humidity. *Sensors* **2022**, *22*, 3301. [[CrossRef](#)]
195. Nair, S.S.; Illyaskutty, N.; Tam, B.; Yazaydin, A.O.; Emmerich, K.; Steudel, A.; Hashem, T.; Schöttner, L.; Wöll, C.; Kohler, H.; et al. ZnO@ZIF-8: Gas sensitive core-shell hetero-structures show reduced cross-sensitivity to humidity. *Sens. Actuators B Chem.* **2020**, *304*, 127184. [[CrossRef](#)]
196. Spagnoli, E.; Fabbri, B.; Gaiardo, A.; Valt, M.; Ardit, M.; Krik, S.; Cruciani, G.; Della Ciana, M.; Vanzetti, L.; Vola, G.; et al. Design of a metal-oxide solid solution for selective detection of ethanol with marginal influence by humidity. *Sens. Actuators B Chem.* **2022**, *370*, 132426. [[CrossRef](#)]
197. Schipani, F.; Miller, D.B.; Ponce, M.A.; Aldao, C.M.; Akbar, S.A.; Morris, P.A. Electrical characterization of semiconductor oxide-based gas sensors using impedance spectroscopy: A review. *Rev. Adv. Sci. Eng.* **2016**, *5*, 86–105. [[CrossRef](#)]
198. Ratan, S.; Kumar, C.; Kumar, A.; Jarwal, D.K.; Mishra, A.K.; Upadhyay, R.K.; Singh, A.P.; Jit, S. Room temperature high hydrogen gas response in Pd/TiO₂/Si/Al capacitive sensor. *Micro Nano Lett.* **2020**, *15*, 632–635. [[CrossRef](#)]
199. Marimuthu, G.; Nguyen, B.S.; Pham, V.T.; Nguyen, V.H.; Tran, V.M.; Sivashanmugan, K.; Pazhanivel, T. Novel NiCo₂O₄/MWCNTs nanocomposite with flake-like architecture as room temperature capacitive-type NH₃ gas sensor. *Mater. Lett.* **2021**, *283*, 128814. [[CrossRef](#)]
200. Schipani, F.; Miller, D.B.; Ponce, M.A.; Aldao, C.M.; Akbar, S.A.; Morris, P.A.; Xu, J. Conduction mechanisms in SnO₂ single-nanowire gas sensors: An impedance spectroscopy study. *Sens. Actuators B Chem.* **2017**, *241*, 99–108. [[CrossRef](#)]
201. Lee, S.; Jin, J.; Baek, J.; Lee, J.; Chae, H. Readout integrated circuit for small-sized and low-power gas sensor based on HEMT device. *Sensors* **2021**, *21*, 5637. [[CrossRef](#)] [[PubMed](#)]
202. Drix, D.; Schmuker, M. Resolving fast gas transients with metal oxide sensors. *ACS Sens.* **2021**, *6*, 688–692. [[CrossRef](#)] [[PubMed](#)]
203. Burgués, J.; Hernandez, V.; Lilienthal, A.J.; Marco, S. Smelling nano aerial vehicle for gas source localization and mapping. *Sensors* **2019**, *19*, 478. [[CrossRef](#)]
204. Acharyya, S.; Jana, B.; Nag, S.; Saha, G.; Guha, P.K. Single resistive sensor for selective detection of multiple VOCs employing SnO₂ hollowspheres and machine learning algorithm: A proof of concept. *Sens. Actuators B Chem.* **2020**, *321*, 128484. [[CrossRef](#)]
205. Liu, T.; Guo, L.; Wang, M.; Su, C.; Wang, D.; Dong, H.; Chen, J.; Wu, W. Review on algorithm design in electronic noses: Challenges, status, and trends. *Intell. Comput.* **2023**, *2*, 0012. [[CrossRef](#)]
206. Casey, J.G.; Collier-Oxandale, A.; Hannigan, M. Performance of artificial neural networks and linear models to quantify 4 trace gas species in an oil and gas production region with low-cost sensors. *Sens. Actuators B Chem.* **2019**, *283*, 504–514. [[CrossRef](#)]

Disclaimer/Publisher’s Note: The statements, opinions and data contained in all publications are solely those of the individual author(s) and contributor(s) and not of MDPI and/or the editor(s). MDPI and/or the editor(s) disclaim responsibility for any injury to people or property resulting from any ideas, methods, instructions or products referred to in the content.